

# Evidence for a Two-Dimensional Quantum Glass State at High Temperatures

Google Quantum AI and collaborators  
(Dated: January 6, 2026)

Disorder in quantum many-body systems can drive transitions between ergodic and non-ergodic phases, yet the nature—and even the existence—of these transitions remains intensely debated [1–11]. Using a two-dimensional array of superconducting qubits, we study an interacting spin model at finite temperature in a disordered landscape, tracking dynamics both in real space and in Hilbert space. Over a broad disorder range, we observe an intermediate non-ergodic regime with glass-like characteristics: physical observables become broadly distributed and some, but not all, degrees of freedom are effectively frozen. The Hilbert-space return probability shows slow power-law decay, consistent with finite-temperature quantum glassiness. In the same regime, we detect the onset of a finite Edwards-Anderson order parameter and the disappearance of spin diffusion. By contrast, at lower disorder, spin transport persists with a nonzero diffusion coefficient. Our results show that there is a transition out of the ergodic phase in two-dimensional systems.

Glassy behavior emerges when a system fails to equilibrate on experimentally relevant timescales, leading to slow relaxation and frozen degrees of freedom [12–14]. Typically this behavior is due to competing interactions (frustration). In quantum systems, disorder and interactions can produce quantum glass phases, characterized by Hilbert space fragmentation, where some degrees of freedom remain frozen while others fluctuate, giving rise to rich non-ergodic dynamics [15]. These phases exhibit hallmark features such as history dependence, slow, power-law relaxation and broadly distributed local observables, distinguishing them from both thermal and fully localized states. Qualitatively, the phase space of classical glasses is separated into an exponentially large number of compartments,  $\mathcal{N}$ , that trap the system. The configurational entropy is extensive,  $S_{\text{conf}} = \ln(\mathcal{N}) \propto n$ , where  $n$  is the number of atoms (spins). In addition, glasses and spin glasses universally exhibit localized two-level systems and related low-frequency  $1/f$ -noise, both of which are understood phenomenologically: although most atoms (spins in spin glass) are locked in their positions, some tunnel between configurations of close energies forming infamous two-level systems and produce the noise [16–18]. Despite phase space compartmentalization, classical glasses display aging and rejuvenation phenomena [19, 20]. This implies the existence of rich dynamics within each phase space compartment of classical glasses. Their quantum analogues are not understood so well. Quantum simulation, as applied in this work, offers the unique possibility to correlate the real space properties of quantum glasses with the properties of the wavefunctions in Hilbert space.

A hallmark of glasses is the breakdown of ergodicity. The transition to non-ergodicity in quantum systems can be studied in the framework of many-body localization (MBL), in which all wavefunctions are completely localized. Numerical and theoretical approaches to studying this transition are well-established [21–26], yet definitive conclusions remain elusive. The original approach [1] focused on the freezing of transport at low temperatures ( $T > 0$ ), whereas most subsequent studies have examined a simplified scenario in the infinite-

temperature limit ( $T \rightarrow \infty$ ). In the absence of a controlled analytical theory for realistic systems, one must rely on numerical simulations, which often yield conflicting results regarding the location—or even the existence—of a transition from an ergodic state to an MBL state with frozen dynamics. Between these extremes, an *intermediate* class of eigenstates—referred to here as Non-Ergodic Extended (NEE)—has been proposed (Fig. 1). In contrast to MBL, where the wavefunction is localized to a small, non-scaling region of the Hilbert space, the NEE wavefunction occupies a very large volume that is still much smaller than the full Hilbert space dimension. Wavefunctions that belong to the same volume form a cluster, while wavefunctions from different clusters are non-overlapping with exponentially small matrix elements between them. The number of these clusters at the same energy,  $\mathcal{N}$ , is exponentially large, with entropy  $S = \ln(\mathcal{N}) \propto n$ ; this matches the configurational entropy of a classical glass. Because the volume of these eigenstates is large, there are many eigenstates within each cluster, and as a result they exhibit a significant overlap that facilitates fast entanglement growth; however, the number of states entangled in this process remains restricted to a small fraction of the total Hilbert space. These distinctive Hilbert space features directly manifest in the transport properties of the system, further distinguishing the NEE phase from the fully localized MBL state. The high Hilbert space connectivity—while insufficient for macroscopic particle transport—provides the necessary channels for energy transport and dephasing, features that are entirely obstructed in a fully localized MBL state. While the field is actively debating the fate of NEE states in the infinite-time and thermodynamic limit (see, e.g., Ref. [27]), their robust presence in theoretical studies across a wide range of models, system sizes, and timescales invites a finite-size experimental study. Such a pursuit might reveal phenomena that fall outside the traditional binary of ergodic and localized phases.

**NEE plausibility.** Crucial for the understanding of classical glasses is the theoretical solution of infinite-range models, which reproduce the extensive configurational entropy of classical glasses below the transition [14]. Sim-

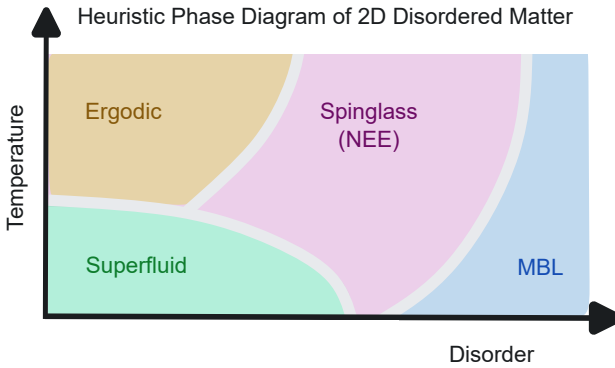


**FIG. 1: Phase Diagram.** At low temperatures and weak disorder, the system exhibits long-range order, while strong disorder localizes the bosons. At high temperatures, weak disorder yields an ergodic diffusive phase; increasing disorder drives a transition to a glassy non-ergodic state with finite Edwards-Anderson order parameter, and ultimately to a fully frozen MBL phase.

ilarly, the existence of NEE states has been convincingly demonstrated in various random matrix models and infinite range systems [28–35]. A key feature of these theoretical models is that the Hamiltonian is a full matrix spanning the entire Hilbert space, with the number of independent random parameters scaling as  $N_r \sim N$ , where  $N$  is the Hilbert-space dimension. In contrast, quantum spin chains and arrays exhibit extreme sparsity in their Hilbert-space Hamiltonians, with  $N_r \sim \ln(N)$ . This sparsity introduces strong correlations between matrix elements, complicating direct application of conventional random matrix frameworks to realistic glasses in 1, 2 or 3 dimensions. In this respect the situation is very similar to the classical theory of (spin) glasses, in which reliable theory is limited to infinite range models [36], which nonetheless provide some qualitative understanding of real glasses.

The peculiarity of many-body quantum systems arises from the exponential growth of Hilbert space volume with the number of local excitation hoppings permitted by the Hamiltonian. In systems with local interactions, this feature separates the criteria for ergodicity and delocalization. Ergodicity requires a state to spread over the *full* Hilbert space allowed by conservation laws, whereas delocalization only demands spreading over a moderately large volume. The distinction between these criteria allows for the existence of an intermediate NEE phase. Early indications of non-ergodic phases in numerical studies appeared as sub-diffusive transport in one-dimensional (1D) models [37–39], as well as in Josephson junction chains [40, 41]. Qualitatively similar features were discussed in Ref. [42] in terms of a pre-thermal regime.

More recently, theoretical arguments supporting NEE states in random spin chains have been presented in the literature [43, 44]. Whether non-ergodic states exist in

many-body systems in more than one spatial dimension ( $D > 1$ ) remains an open and debated question. Several works have argued against the stability of MBL phases in higher dimensions [24, 45–47]. However, these arguments do not rule out a breakdown of ergodicity, as the absence of an MBL phase does not preclude NEE behavior. Generally, numerical simulations of quantum glasses in the NEE state are very difficult because of the exponential volume of the relevant Hilbert space involved.

Recent advances in controllable quantum processors [48] have enabled numerous studies of ergodicity and its breakdown. Most MBL investigations have focused on inferring the phenomenology in real space, particularly by studying the relaxation rates and the asymptotic behavior of population imbalance [49–53]. These experiments are demanding in terms of the number of disorder realizations and repetitions required, readily adding up to  $\sim 10^{10} - 10^{12}$  shots. Superconducting qubit arrays make it possible to directly probe complex dynamics in Hilbert space with fast data rates of tens of kHz [54]. In this work, by studying the dynamics both in Hilbert space and in the real (2D) domain, we find evidence for the existence of an NEE state in spin dynamics with strong disorder at  $T = \infty$ .

The dynamics of excitations in a 2D nearest-neighbor qubit array can be modeled by the spin Hamiltonian

$$H = -J \sum_{\langle i,j \rangle} (S_i^+ S_j^- + S_i^- S_j^+) + \sum_i h_i S_i^z, \quad (1)$$

where  $S_i^\alpha$  are spin- $\frac{1}{2}$  operators,  $h_i$  are site-dependent random disorder drawn from a box distribution of width  $W$  and zero mean, and  $J$  denotes the nearest-neighbor coupling strength on the square spin lattice. The competing interactions in this case are XY coupling, which favours long-range XY order, and an applied field in the Z direction. Building on prior studies and general physical considerations, a phase diagram of this interacting spin model can be proposed, as shown in Fig. 1. At low temperature and weak disorder, the system exhibits long-range order, corresponding to superfluidity of hardcore bosons. Large-scale quantum Monte Carlo  $T = 0$  simulations [55] confirm superfluidity at weaker disorder,  $w \equiv W/J \leq 19$ , beyond which bosons become localized. Further increasing disorder drives the system into a glassy, non-ergodic phase characterized by a nonzero Edwards-Anderson order parameter.

**Glassy behavior in magnetization.** We begin our experimental studies by measuring the local magnetization in real space, a quantity that is readily accessible on most quantum processors. Starting from a 59-qubit product state at  $t = 0$ , we consider the relaxation of the spin distributions, shown in Fig. 2a for two different disorder strengths,  $w = 9$  and  $w = 15$ . The subsequent spatial maps show that the magnetization profile relaxes almost completely in the case of low disorder ( $w = 9$ ), whereas substantial magnetization remains frozen at higher dis-

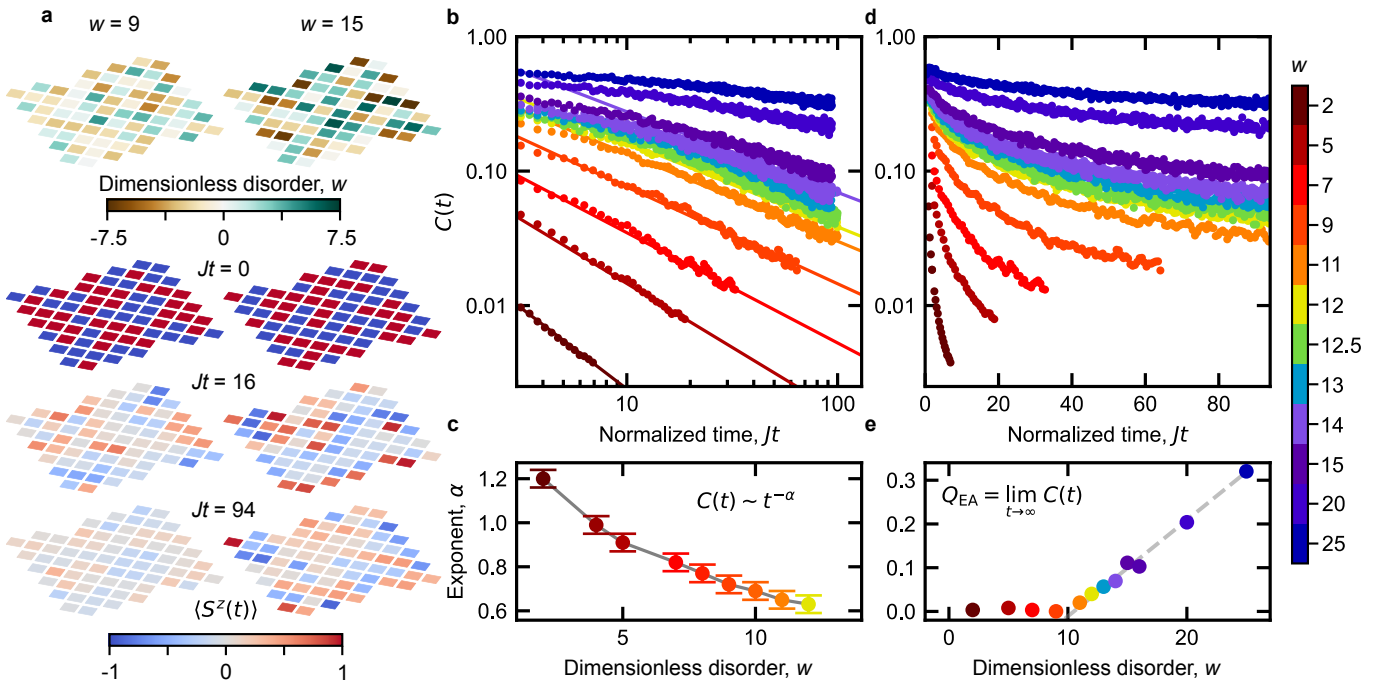


**FIG. 2: Evidence of glass formation in the frozen magnetization.** **a**, Temporal evolution of magnetization for disorders of  $w = 9$  and  $w = 15$  (corresponding disorder patterns showed on top), revealing slower relaxation at the higher disorder. **b**, Time dependence of the spin glass correlation function  $C(t)$ , showing power law relaxation of  $C(t)$  in the ergodic phase. **c**, Disorder-dependence of the dynamic exponent  $\alpha$  that describes the power-law decay of  $C(t)$ . **d**, Same as **b**, but with linear axis, revealing the absence of complete relaxation at higher disorders. **e**, The Edwards-Anderson order parameter,  $Q_{EA} = C(\infty)$ , as a function of  $w$  shows an abrupt change in slope near  $w = w_c \simeq 10$ .  $Q_{EA}$  is extracted from fitting  $C(t)$  with a decaying functional form (exponential with or without a power-law prefactor, see SI) with a constant offset.

order ( $w = 15$ ). This is a first indication of reduced ergodicity. To further study this contrasting behavior, we next plot the dynamic spin-glass correlation function,

$$C(t) = \overline{\langle S_i^z(0) S_i^z(t) \rangle^2}, \quad (2)$$

for a wide range of disorder values (Fig. 2b). In the weakly disordered regime, the correlation function is found to agree well with a power-law decay, with an exponent  $\alpha$  that decreases from unity to about  $2/3$  as  $w$  approaches a critical value,  $w_c \sim 10$  (Fig. 2c). Beyond this point, however, the correlation decay deviates from power-law behavior (see further analysis in SI) and saturates at a non-zero value of the Edwards-Anderson order parameter,  $Q_{EA} = C(t \rightarrow \infty)$ , as is more clearly observed with a linear time axis (Fig. 2d). This behavior is quantified in Fig. 2e, where we show the extracted  $Q_{EA}$ : while  $Q_{EA}$  is found to be very small in the ergodic regime, we observe a clear change to linear growth with disorder for  $w \gtrsim 11$ , consistent with a transition or sharp cross-over. The observed freezing-in of magnetization dynamics is in qualitative agreement with earlier observations [50].

**Return probability.** While the real-space magnetization dynamics have provided valuable information about disorder-induced slowdown in previous studies [52, 53] and have enabled us to characterize the  $w$ -dependence

of  $Q_{EA}$ , their ability to fully characterize the disordered regime is limited. Moreover, drawing definite conclusions has previously been made challenging by small values of the decay exponents ( $10^{-2} - 10^{-1}$ ) and thus modest variation over available experimental timescales [52, 53]. Hence, to gain a more comprehensive picture, we move beyond these real-space metrics to probe the system's dynamics in Hilbert space by measuring the return probability,

$$R(t) = |\langle \Psi(t) | \Psi(0) \rangle|^2, \quad (3)$$

which quantifies ergodic behavior in Hilbert space: in an ergodic system, the probability of returning to the initial state should quickly drop to the inverse number of states allowed by conservation laws. The measurement sequence proceeds as follows: (i) prepare an initial state in the form of a bit-string—an eigenstate of all  $S_i^z$  operators—corresponding to a total energy near the middle of the energy spectrum; (ii) evolve the system under the Hamiltonian for time  $t$ ; (iii) measure in the same basis. Typical instances are shown for  $w = 9$  and  $w = 15$  in Fig. 3a: while many spins flip after a short amount of time for  $w = 9$ , only a few spins flip in the case of larger disorder. These pairs form effective two-level systems.

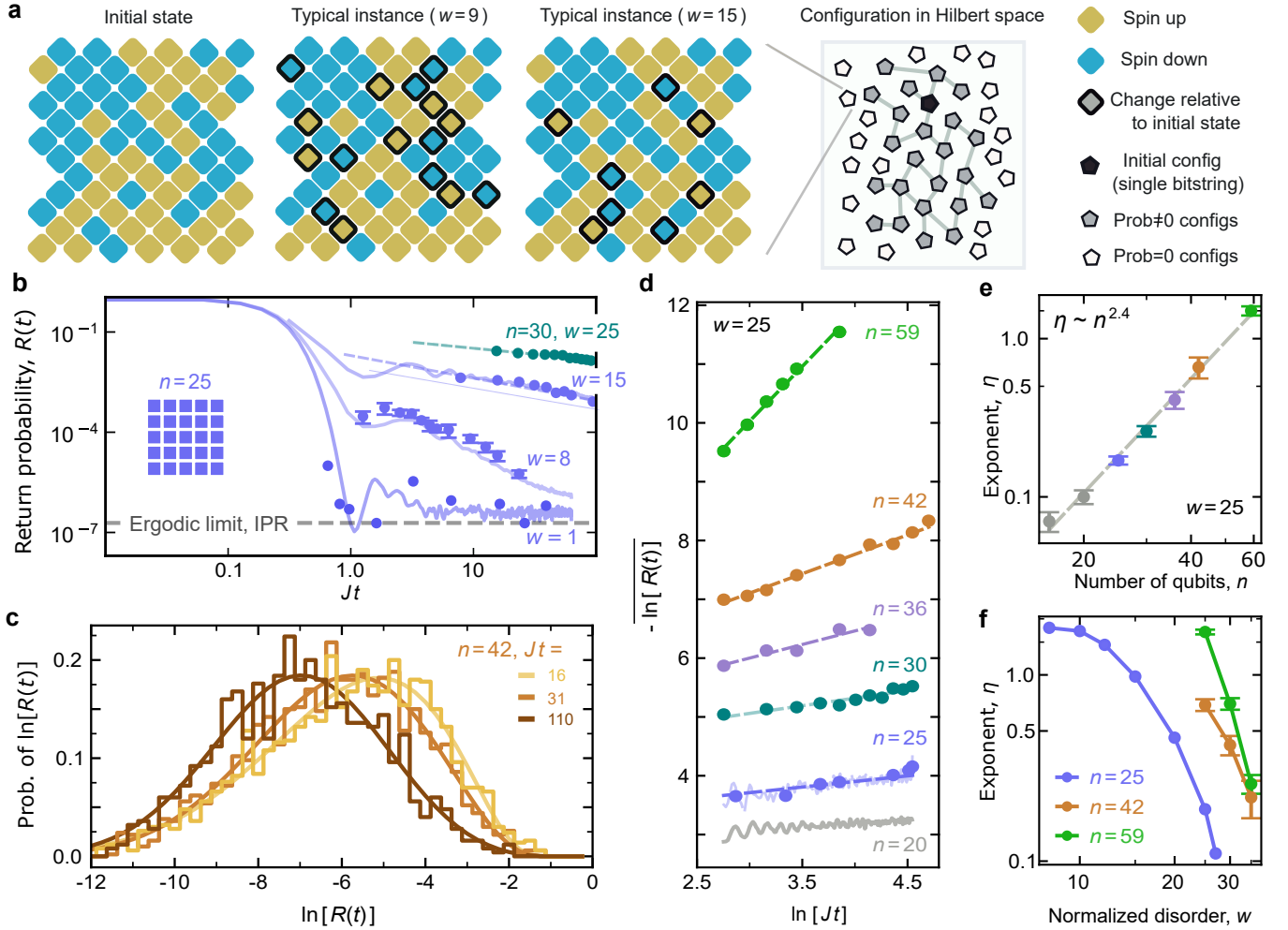


**FIG. 3: Signatures of glassy behavior in the return probability.** **a**, Real-space measurement instances show that fewer spins are flipped when  $w$  is higher. The return probability is defined as the fraction of the measurements in which no spins are flipped. **b**, Time dependence of measured return probability for  $n = 25$  (circles), which shows a local minimum ("correlation hole") at low disorder, and power-law decay for larger  $w$ . Solid curves show results from exact numerical modeling, averaged over  $\sim 2500$  disorder instances (100 for  $w = 1$ ), while straight lines indicate power-law fits. **c**, Return probability on logarithmic scales shows a wide distribution, for  $n = 42$  and at three different evolution times ( $w = 30$ ). Solid lines are Gaussian fits. **d**, Time dependence of return probability  $R(t)$  for a range of system sizes, displaying power-law dependence on time for  $w = 25$ . Solid straight lines show power-law fits. **e**, The power-law exponents extracted in **d** scale as  $\eta \propto n^{2.4}$ . **f**, Exponent  $\eta$  as a function of disorder for different system sizes. Continuous lines in panel **d**,  $n = 20, 25$ , as well as grey symbols in panel **e**,  $n = 16, 20$  show results of numerical simulations; for  $n = 25$  numerical results coincide with experimental ones.

To obtain the return probability  $R(t)$ , steps (i)–(iii) are repeated  $10^5$ – $10^6$  times for a given  $\Psi(0)$ . The measured  $R(t)$  depends on both the initial state  $\Psi(0)$  and the realization of the random fields  $h_i$ . To determine its probability distribution, we averaged over many initial bit-strings and randomized field configurations—typically  $\sim 10^3$  realizations in the non-ergodic regime.

In the ergodic phase ( $w = 1$ ),  $R(t)$  is found to quickly decay to a very small value, which is the inverse of the total size of available Hilbert-space, i.e.  $1/N = \binom{n}{n/2}^{-1} \sim 2^{-n}$ . Before reaching that asymptotic value,  $R(t)$  shows

a shallow minimum around  $Jt \sim 1$ , consistent with a "correlation hole" [56, 57]. Note that resolving the small return probabilities in this regime ( $w = 1$ ) requires a very large number of shots ( $\sim 10^8$ ), making averaging over disorder very difficult. At larger disorders,  $w > w_c \simeq 10$ , corresponding to non-ergodic phase, the correlation hole disappears and the return probability begins to hint at power-law dependence,

$$R_{\text{typ}}(t) \sim (Jt)^{-\eta} \quad (4)$$

At the same time the return probability at any given

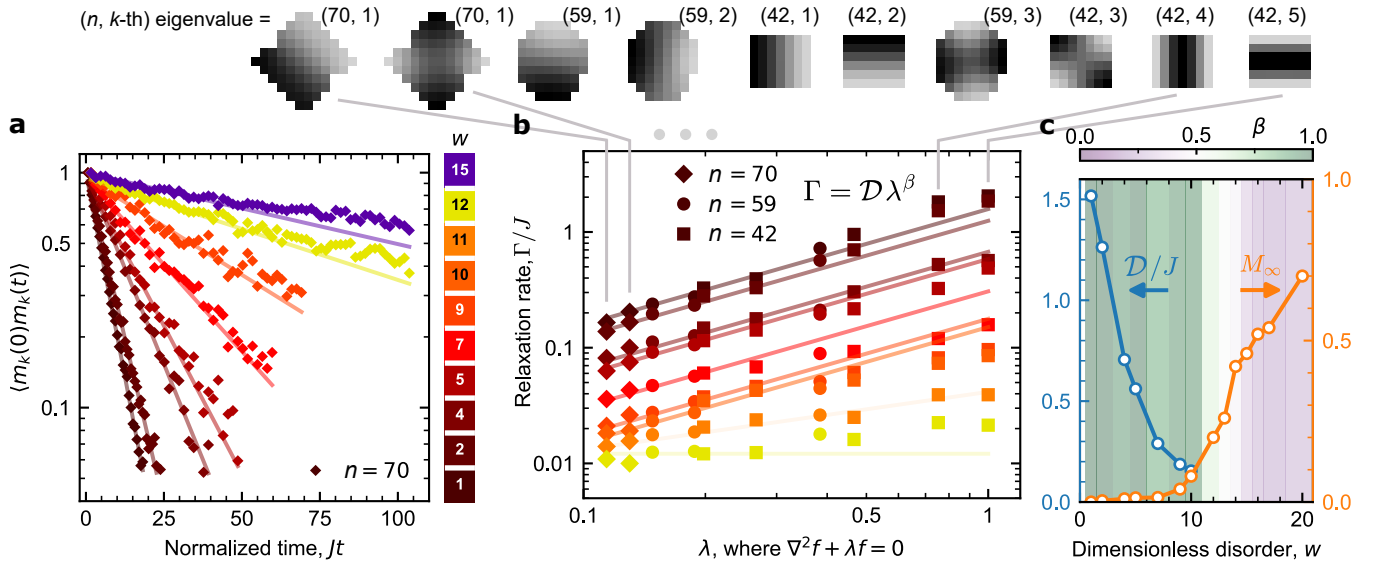


**FIG. 4: Disappearance of diffusion at strong disorder.** **a**, The measured relaxation of magnetization  $\langle m_k(t) m_k(0) \rangle$  for the smallest eigenmode ( $k = 1$ ) at several values of disorder ( $n = 70$ ). **b**, Extracted relaxation rates for  $n = 42, 59$  and  $70$ . Solid lines are fits using  $\Gamma = \mathcal{D} \lambda^\beta$ . **c**, The extracted diffusion constant  $\mathcal{D}$  (left axis) and non-zero frozen amplitude  $M_\infty$  (right axis). Background colors denote  $\beta$ , resulting from fitting data in **b** with  $\Gamma = \mathcal{D} \lambda^\beta$ . Diffusion applies for  $\beta \approx 1$  and fails as  $\beta$  departs from unity and hence  $\mathcal{D}$  cannot be extracted above  $w > 10$ .

time acquires a very wide distribution, even on the logarithmic scale (Fig. 3c). Hence, we fit the distribution of  $\ln(R)$  with Gaussians to obtain the dependence of the typical  $\ln R(t)$  on system size, shown in Fig. 3d. We observe that the decay of the typical return probability is consistent with a power-law for all system sizes considered in the experiment. Importantly, the exponent  $\eta$  is found to grow superlinearly with  $n$ ,

$$\eta \approx \kappa(w) \cdot n^{2.4}, \quad (5)$$

as plotted in Fig. 3e for  $w = 30$ . At large  $w$  the exponent  $\eta$  decreases quickly (Fig. 3f), suggesting the appearance of a more localized phase at higher disorders.

This behavior of  $R_{\text{typ}}$  is consistent with residual interactions between different spin pairs leading to dephasing and inelastic transitions (see also Supplement). Power-law decay of  $R_{\text{typ}}$  at long times suggests that the probability for a flip of any spin  $S_i^\alpha$  of the array grows logarithmically with time like  $P_{\text{flip}} \sim (\eta/n) \ln(Jt)$ ; this behavior generates spin noise with a  $1/f$  power spectrum, known to be generic for glasses and spin glasses (see Supplement for supporting numerical simulations). Crucially, the noise power spectrum depends on the number of active spin pairs, resulting in a superlinear dependence of  $\eta(n)$ , as observed experimentally. Since non-interacting pairs would typically produce a linear scaling, this superlinearity supports the conclusion that the dephasing arises from internal dynamics rather than external noise.

The observed power-law decay of  $R_{\text{typ}}$  at moderately strong disorder,  $10 \leq w \leq 35$ , is consistent with nu-

merical results in 1D [58] (see Supplement), and differs qualitatively from both the oscillatory behavior around a large value expected in the fully localized MBL phase and the exponentially fast decay to very low values in the ergodic phase.

**Breakdown of diffusion.** In the presence of locally conserved quantities, relaxation of an ergodic state can be characterized by how each conserved quantity diffuses. Figure 4a shows the relaxation of the magnetization correlations,  $\langle m_{k=1}(t) m_{k=1}(0) \rangle$ , for various disorder strengths, after projecting (in post-processing) onto the longest-wavelength eigenmode of the diffusion operator,  $-\nabla^2$ , for the qubit system (computed for the actual lattice shape, e.g.  $\lambda_{\min} = 0.114$  for  $n = 70$ ). At weak disorder ( $w = 1, 2, 4$ ), the magnetization decays exponentially as  $\propto e^{-\Gamma t}$ . For moderate disorder ( $w = 5, 7, 9$ ), the relaxation becomes slower, pointing to the onset of anomalous diffusion. At strong disorder, the decay is slower than exponential at long times, and the magnetization does not fully vanish; even at the longest time scales, a finite remnant amplitude  $M_\infty$  persists. An “effective” relaxation rate  $\Gamma$  can still be defined from the short-time slope of the relaxation curve. Fig. 4b shows the fitted  $\Gamma$  versus the Laplacian eigenvalue,  $\lambda$ , for several disorder strengths and three different system sizes of  $42, 59$  and  $70$  qubits (50 – 100 disorder realizations for each case), which show good agreement for similar values of  $\lambda$ . At low disorder,  $\Gamma$  scales linearly with the eigenvalue up to  $\lambda \approx 0.5$ , consistent with normal diffusion with diffusion constant,  $\mathcal{D}$ . At stronger disorder, this proportionality

weakens and eventually breaks down. Fig. 4c summarizes the extracted diffusion constant  $\mathcal{D}$  versus disorder strength, showing that near a critical value  $w \simeq 10$ ,  $\mathcal{D}$  drops to  $\mathcal{D} \sim 0.1$ , while a finite residual magnetization  $M_\infty$  emerges for  $w > w_c$ . In this panel we also show the value of  $\beta$  resulting from fitting  $\Gamma = a\lambda^\beta$ ; as expected,  $\beta \approx 1$  in the ergodic phase but drops for  $w > w_c$ .

Quantum glass phases are particularly interesting from a computational perspective, as their non-universal dynamics challenge classical descriptions and require exponentially costly simulations. Ergodic states of quantum matter often exhibit a substantial degree of universality that depends only weakly on the specifics of the Hamiltonian, a property that frequently makes them more accessible to study via classical computational methods. MBL states—characterized by the existence of local integrals of motion (LIOMs)—have in some regimes been handled using perturbative treatments starting from a fully frozen limit, making them more classically tractable [59]. The dynamics of a quantum system in a NEE phase, however, carry specific non-universal features tied to a particular disorder realization, thus limiting the efficacy of semi-classical Boltzmann approaches involving disorder averaging. Moreover, the NEE phase does not support LIOMs, which makes it more challenging to approach with convergent perturbative approaches based on MBL-like approximations. Direct quantum simulation is uniquely suited to study such systems, enabling extraction of key dynamical fingerprints and thereby a sensitive probe of the Hamiltonian parameters.

In this work, by measuring return probabilities in both Hilbert and real space, we found evidence for non-ergodic—though not fully localized—dynamics at high-temperatures in a prototypical 2D disordered array of interacting spins. This behavior spans a broad range of disorder strengths and serves as an analog of low-temperature spin glasses. The absence of spin diffusion in this glassy phase does not imply frozen energy transport. On the contrary, we expect energy to propagate throughout the phase via power-law decay, distinguishing it qualitatively from a fully localized MBL state. Our theoretical analysis (see Supplement) indicates that the glassy phase is characterized by a single-spin dephasing rate,  $\Gamma_\phi$ , typically much larger than the relaxation rate,  $\Gamma_r$ —a likely generic feature of strongly disordered systems with local interactions. This dephasing slowly suppresses interferences and leads to irreversibility of the dynamics. At very strong disorder, the power-law exponent rapidly approaches zero for all accessible system sizes, suggesting a transition to a many-body-localized phase without transport. The same MBL phase might also emerge at somewhat weaker disorder in low-temperature regimes. Although we here consider system sizes of up to 70 qubits, this does not guarantee that we have reached the true asymptotic regime. The same holds for the accessible time window ( $Jt \leq 100$ ). While these limitations prevent direct access to the strict thermodynamic limit, studies at these experimentally relevant scales already

provide valuable insight into the physics of real quantum systems.

<sup>†</sup> Google Quantum AI and Collaborators

A. Lunkin<sup>1,‡</sup>, N. S. Ticea<sup>2,3,‡</sup>, S. Kumar<sup>2,4</sup>, C. Miao<sup>2,5</sup>, J. Choi<sup>2,6</sup>, M. Alghadeer<sup>2,7</sup>, I. Drozdov<sup>2,8</sup>, D. Abanin<sup>2</sup>, A. Abbas<sup>2</sup>, R. Acharya<sup>2</sup>, L. Aghababaie Beni<sup>2</sup>, G. Aigeldinger<sup>2</sup>, R. Alcaraz<sup>2</sup>, S. Alcaraz<sup>2</sup>, M. Ansmann<sup>2</sup>, F. Arute<sup>2</sup>, K. Arya<sup>2</sup>, W. Askew<sup>2</sup>, N. Astrakhantsev<sup>2</sup>, J. Atalaya<sup>2</sup>, R. Babbush<sup>2</sup>, B. Ballard<sup>2</sup>, J. C. Bardin<sup>2,9</sup>, H. Bates<sup>2</sup>, A. Bengtsson<sup>2</sup>, M. Bigdeli Karimi<sup>2</sup>, A. Bilmes<sup>2</sup>, S. Bilodeau<sup>2</sup>, F. Borjans<sup>2</sup>, A. Bourassa<sup>2</sup>, J. Bovaird<sup>2</sup>, D. Bowers<sup>2</sup>, L. Brill<sup>2</sup>, P. Brooks<sup>2</sup>, M. Broughton<sup>2</sup>, D. A. Browne<sup>2</sup>, B. Buchea<sup>2</sup>, B. B. Buckley<sup>2</sup>, T. Burger<sup>2</sup>, B. Burkett<sup>2</sup>, N. Bushnell<sup>2</sup>, J. Busnaina<sup>2</sup>, A. Cabrera<sup>2</sup>, J. Campero<sup>2</sup>, H.-S. Chang<sup>2</sup>, S. Chen<sup>2</sup>, Z. Chen<sup>2</sup>, B. Chiaro<sup>2</sup>, L.-Y. Chih<sup>2</sup>, A. Y. Cleland<sup>2</sup>, B. Cochran<sup>2</sup>, M. Cockrell<sup>2</sup>, J. Cogan<sup>2</sup>, R. Collins<sup>2</sup>, P. Conner<sup>2</sup>, H. Cook<sup>2</sup>, R. G. Cortinas<sup>2</sup>, W. Courtney<sup>2</sup>, A. L. Crook<sup>2</sup>, B. Curtin<sup>2</sup>, M. Damyanov<sup>2</sup>, S. Das<sup>2</sup>, D. M. Debroy<sup>2</sup>, S. Demura<sup>2</sup>, P. Donohoe<sup>2</sup>, A. Dunsworth<sup>2</sup>, V. Ehimhen<sup>2</sup>, A. Eickbusch<sup>2</sup>, A. Moshe Elbag<sup>2</sup>, L. Ella<sup>2</sup>, M. Elzouka<sup>2</sup>, D. Enriquez<sup>2</sup>, C. Erickson<sup>2</sup>, L. Faoro<sup>2</sup>, V. S. Ferreira<sup>2</sup>, M. Flores<sup>2</sup>, L. Flores Burgos<sup>2</sup>, S. Fontes<sup>2</sup>, E. Forati<sup>2</sup>, J. Ford<sup>2</sup>, B. Foxen<sup>2</sup>, M. Fukami<sup>2</sup>, A. Wing Lun Fung<sup>2</sup>, L. Fuste<sup>2</sup>, S. Ganjam<sup>2</sup>, G. Garcia<sup>2</sup>, C. Garrick<sup>2</sup>, R. Gasca<sup>2</sup>, H. Gehring<sup>2</sup>, R. Geiger<sup>2</sup>, E. Genois<sup>2</sup>, W. Giang<sup>2</sup>, D. Gilboa<sup>2</sup>, J. E. Goeders<sup>2</sup>, E. C. Gonzales<sup>2</sup>, R. Gosula<sup>2</sup>, S. J. de Graaf<sup>2</sup>, A. Grajales Dau<sup>2</sup>, D. Graumann<sup>2</sup>, J. Grebel<sup>2</sup>, A. Greene<sup>2</sup>, J. A. Gross<sup>2</sup>, J. Guerrero<sup>2</sup>, L. Le Guevel<sup>2</sup>, T. Ha<sup>2</sup>, S. Habegger<sup>2</sup>, T. Hadick<sup>2</sup>, A. Hadjikhani<sup>2</sup>, M. C. Hamilton<sup>2,14</sup>, M. Hansen<sup>2</sup>, M. P. Harrigan<sup>2</sup>, S. D. Harrington<sup>2</sup>, J. Hartshorn<sup>2</sup>, S. Heslin<sup>2</sup>, P. Heu<sup>2</sup>, O. Higgott<sup>2</sup>, R. Hiltermann<sup>2</sup>, J. Hilton<sup>2</sup>, H.-Y. Huang<sup>2</sup>, M. Hucka<sup>2</sup>, C. Hudspeth<sup>2</sup>, A. Huff<sup>2</sup>, W. J. Huggins<sup>2</sup>, E. Jeffrey<sup>2</sup>, S. Jevons<sup>2</sup>, Z. Jiang<sup>2</sup>, X. Jin<sup>2</sup>, C. Jones<sup>2</sup>, C. Joshi<sup>2</sup>, P. Juhas<sup>2</sup>, A. Kabel<sup>2</sup>, D. Kafri<sup>2</sup>, H. Kang<sup>2</sup>, K. Kang<sup>2</sup>, A. H. Karamlou<sup>2</sup>, R. Kaufman<sup>2</sup>, K. Kechedzhii<sup>2</sup>, J. Kelly<sup>2</sup>, T. Khattar<sup>2</sup>, M. Khezri<sup>2</sup>, S. Kim<sup>2</sup>, P. V. Klimov<sup>2</sup>, C. M. Knaut<sup>2</sup>, B. Kobrin<sup>2</sup>, A. N. Korotkov<sup>2</sup>, F. Kostritsa<sup>2</sup>, J. M. Kreikebaum<sup>2</sup>, R. Kudo<sup>2</sup>, B. Kueffler<sup>2</sup>, A. Kumar<sup>2</sup>, V. D. Kurilovich<sup>2</sup>, V. Kutsko<sup>2</sup>, D. Landhuis<sup>2</sup>, T. Lange-Del<sup>2</sup>, B. W. Langley<sup>2</sup>, P. Laptev<sup>2</sup>, K.-M. Lau<sup>2</sup>, E. Leavell<sup>2</sup>, J. Ledford<sup>2</sup>, J. Lee<sup>2</sup>, K. Lee<sup>2</sup>, B. J. Lester<sup>2</sup>, W. Leung<sup>2</sup>, L. Li<sup>2</sup>, W. Yan Li<sup>2</sup>, M. Li<sup>2</sup>, A. T. Lill<sup>2</sup>, W. P. Livingston<sup>2</sup>, M. T. Lloyd<sup>2</sup>, L. de Lorenzo<sup>2</sup>, E. Lucero<sup>2</sup>, D. Lundahl<sup>2</sup>, A. Lunt<sup>2</sup>, S. Madhuk<sup>2</sup>, A. Maiti<sup>2</sup>, A. Malone<sup>2</sup>, S. Mandrà<sup>2</sup>, L. S. Martin<sup>2</sup>, O. Martin<sup>2</sup>, E. Mascot<sup>2</sup>, P. Masih Das<sup>2</sup>, D. Maslov<sup>2</sup>, M. Mathews<sup>2</sup>, C. Maxfield<sup>2</sup>, J. R. McClean<sup>2</sup>, M. McEwen<sup>2</sup>, S. Meeks<sup>2</sup>, A. Megrant<sup>2</sup>, K. C. Miao<sup>2</sup>, Z. K. Minev<sup>2</sup>, R. Molavi<sup>2</sup>, S. Molina<sup>2</sup>, S. Montazeri<sup>2</sup>, C. Neill<sup>2</sup>, M. Newman<sup>2</sup>, A. Nguyen<sup>2</sup>, M. Nguyen<sup>2</sup>, C.-H. Ni<sup>2</sup>, M. Y. Niu<sup>2</sup>, L. Oas<sup>2</sup>, W. D. Oliver<sup>2</sup>, R. Orosco<sup>2</sup>, K. Ottosson<sup>2</sup>, A. Pagano<sup>2</sup>, A. Di Paolo<sup>2</sup>, S. Peek<sup>2</sup>, D. Peterson<sup>2</sup>, A. Pizzuto<sup>2</sup>, E. Portoles<sup>2</sup>, R. Potter<sup>2</sup>, O. Pritchard<sup>2</sup>, M. Qian<sup>2</sup>, C. Quintana<sup>2</sup>, G. Ramachandran<sup>2</sup>, A. Ranadive<sup>2</sup>, M. J. Reagor<sup>2</sup>, R. Resnick<sup>2</sup>, D. M. Rhodes<sup>2</sup>, D. Riley<sup>2</sup>, G. Roberts<sup>2</sup>, R. Rodriguez<sup>2</sup>, E. Ropes<sup>2</sup>, L. B. De Rose<sup>2</sup>, E. Rosenberg<sup>2</sup>, E. Rosenfeld<sup>2</sup>, D. Rosenstock<sup>2</sup>, E. Rossi<sup>2</sup>, D. A. Rower<sup>2</sup>, R. Salazar<sup>2</sup>, K. Sankaragomathi<sup>2</sup>, M. Can Sarihan<sup>2</sup>, K. J. Satzinger<sup>2</sup>, M. Schaefer<sup>2,10</sup>, S. Schroeder<sup>2</sup>, H. F. Schurkus<sup>2</sup>, A. Shahingohar<sup>2</sup>, M. J. Shearn<sup>2</sup>, A. Shorter<sup>2</sup>, V. Shvarts<sup>2</sup>, V. Sivak<sup>2</sup>, S. Small<sup>2</sup>, W. Clarke Smith<sup>2</sup>, D. A. Sobel<sup>2</sup>, B. Spells<sup>2</sup>, S. Springer<sup>2</sup>, G. Sterling<sup>2</sup>, J. Suchard<sup>2</sup>, A. Szasz<sup>2</sup>, A. Sztein<sup>2</sup>, M. Taylor<sup>2</sup>, J. P. Thiruraman<sup>2</sup>, D. Thor<sup>2</sup>, D. Timucin<sup>2</sup>, E. Tomita<sup>2</sup>, A. Torres<sup>2</sup>, M. Mert Torunbalci<sup>2</sup>, H. Tran<sup>2</sup>, A. Vaishnav<sup>2</sup>, J. Vargas<sup>2</sup>, S. Vdovichev<sup>2</sup>, G. Vidal<sup>2</sup>, B. Villalonga<sup>2</sup>, C. Vollgraff Heidweiller<sup>2</sup>, M. Voorhees<sup>2</sup>, S. Waltman<sup>2</sup>, J. Waltz<sup>2</sup>, S. X. Wang<sup>2</sup>, B. Ware<sup>2</sup>, J. D. Watson<sup>2</sup>, Y. Wei<sup>2</sup>, T. Weidel<sup>2</sup>, T. White<sup>2</sup>, K. Wong<sup>2</sup>, B. W. K. Woo<sup>2</sup>, C. J. Wood<sup>2</sup>, M. Woodson<sup>2</sup>, C. Xing<sup>2</sup>, Z. Jamie Yao<sup>2</sup>, P. Yeh<sup>2</sup>, B. Ying<sup>2</sup>, J. Yoo<sup>2</sup>, N. Yosri<sup>2</sup>, E. Young<sup>2</sup>, G. Young<sup>2</sup>, A. Zalcman<sup>2</sup>, R. Zhang<sup>2</sup>, Y. Zhang<sup>2</sup>, N. Zhu<sup>2</sup>, N. Zobrist<sup>2</sup>, Z. Zou<sup>2</sup>, S. Boixo<sup>2</sup>, H. Neven<sup>2</sup>, V. Smelyanskiy<sup>2</sup>, T. I. Andersen<sup>2</sup>, P. Roushan<sup>2</sup>, M. V. Feigel'man<sup>1,15,§</sup>, L. B. Ioffe<sup>2,§</sup>

1 Nanocenter CENN, Ljubljana, Slovenia

2 Google Research, Mountain View, CA, USA

3 Department of Applied Physics, Stanford University, Stanford, California 94305, USA

4 Department of Electrical and Computer Engineering, Princeton University, Princeton, NJ, USA

5 Department of Physics, Stanford University, Stanford California 94305, USA

6 School of Applied and Engineering Physics, Cornell University, Ithaca, New York 14853, USA

7 Department of Physics, Clarendon Laboratory, University of Oxford, OX1 3PU, UK

8 Department of Physics, University of Connecticut, Storrs, CT

9 Department of Electrical and Computer Engineering, University of Massachusetts, Amherst, MA

10 Department of Physics, University of California, Santa Barbara, CA

11 Department of Electrical and Computer Engineering, University of California, Riverside, CA

12 Pritzker School of Molecular Engineering, University of Chicago, Chicago, IL

13 Department of Physics and Astronomy, University of California, Riverside, CA

14 Department of Electrical and Computer Engineering, Auburn University, Auburn, AL

15 Jožef Stefan Institute, Ljubljana, Slovenia

<sup>‡</sup> These authors contributed equally to this work.

<sup>§</sup> Corresponding authors: Mikhail.Feigelman@nanocenter.si and ioffel@google.com

---

[1] D. M. Basko, I. L. Aleiner, and B. L. Altshuler, Metal-insulator transition in a weakly interacting many-electron system with localized single-particle states, *Annals of Physics* **321**, 1126 (2006).

[2] E. Altman and R. Vosk, Universal dynamics and renormalization in many-body-localized systems, *Annu. Rev. Condens. Matter Phys.* **6**, 383 (2015).

[3] R. Nandkishore and D. A. Huse, Many-body localization and thermalization in quantum statistical mechanics, *Annu. Rev. Condens. Matter Phys.* **6**, 15 (2015).

[4] D. J. Luitz and Y. B. Lev, The ergodic side of the many-body localization transition, *Annalen der Physik* **529**, 1600350 (2017).

[5] F. Alet and N. Laflorencie, Many-body localization: An introduction and selected topics, *Comptes Rendus Physique* **19**, 498 (2018).

[6] S. Gopalakrishnan and D. A. Huse, Instability of many-body localized systems as a phase transition in a non-standard thermodynamic limit, *Physical Review B* **99**, 134305 (2019).

[7] D. A. Abanin *et al.*, Colloquium: Many-body localization, thermalization, and entanglement, *Rev. Mod. Phys.*

**91**, 021001 (2019).

[8] J. Suntajs, J. Bonča, T. Prosen, and L. Vidmar, Quantum chaos challenges many-body localization, *Physical Review E* **102**, 062144 (2020).

[9] D. Sels and A. Polkovnikov, Dynamical obstruction to localization in a disordered spin chain, *Physical Review E* **104**, 054105 (2021).

[10] J. C. Peacock and D. Sels, Many-body delocalization from embedded thermal inclusion, *Physical Review B* **108**, L020201 (2023).

[11] P. Sierant, M. Lewenstein, A. Scardicchio, L. Vidmar, and J. Zakrzewski, Many-body localization in the age of classical computing, *Reports on Progress in Physics* **88**, 026502 (2025).

[12] S. F. Edwards and P. W. Anderson, Theory of spin glasses, *Journal of Physics F: Metal Physics* **5**, 965 (1975).

[13] K. Binder and A. P. Young, Spin glasses: Experimental facts, theoretical concepts, and open questions, *Reviews of Modern Physics* **58**, 801 (1986).

[14] M. Mézard, G. Parisi, and M. A. Virasoro, *Spin Glass Theory and Beyond* (World Scientific, 1987).

[15] P. Charbonneau, E. Marinari, G. Parisi, F. Ricci-Tersenghi, G. Sicuro, F. Zamponi, and M. Mezard, *Spin glass theory and far beyond: replica symmetry breaking after 40 years* (World Scientific, 2023).

[16] P. Esquinazi, *Tunneling systems in amorphous and crystalline solids* (Springer - Verlag, Berlin Heidelberg New York, 1998).

[17] S. Kogan, *Electronic Noise and Fluctuations in Solids* (Cambridge University Press, 2008).

[18] E. Paladino *et al.*, 1/f noise: implications for solid-state quantum information, *Rev. Mod. Phys.* **86**, 361 (2014).

[19] J.-P. Bouchaud, L. F. Cugliandolo, J. Kurchan, and M. Mezard, "Out of Equilibrium dynamics in Spin-Glasses and other Glassy Systems", in "Spin Glasses and Random Fields", ed. A.P. Young, World Scientific (1998).

[20] E. Vincent, "Ageing, Rejuvenation and Memory: The Example of Spin Glasses", in "Ageing and the Glass Transition", eds. M. Henkel, M. Pleimling and R. Sanctuary, Springer, Berlin Heidelberg (2009).

[21] W. De Roeck, L. Giacomini, F. Huveneers, and O. Prosnik, Absence of normal heat conduction in strongly disordered interacting quantum chains, arXiv preprint arXiv:2408.04338 (2024).

[22] J. Z. Imbrie, On many-body localization for quantum spin chains, *Journal of Statistical Physics* **163**, 998 (2016).

[23] A. Pal and D. A. Huse, Many-body localization phase transition, *Physical Review B—Condensed Matter and Materials Physics* **82**, 174411 (2010).

[24] E. V. Doggen *et al.*, Slow many-body delocalization beyond one dimension, *Phys. Rev. Lett.* **125**, 155701 (2020).

[25] J. Li, A. Chan, and T. B. Wahl, Quantum circuits reproduce the experimental two-dimensional many-body localization transition point, *Phys. Rev. B* **109**, L140202 (2024).

[26] J. Li, A. Chan, and T. B. Wahl, Two-dimensional many-body localized systems coupled to a heat bath, *Phys. Rev. B* **111**, 224211 (2025).

[27] K. Tikhonov and A. Mirlin, Statistics of eigenstates near the localization transition on random regular graphs, *Physical Review B* **99**, 024202 (2019).

[28] V. E. Kravtsov, I. M. Khaymovich, E. Cuevas, and M. Amini, A random matrix model with localization and ergodic transitions, *New J. Phys.* **17**, 122002 (2015).

[29] G. D. Tomasi *et al.*, Survival probability in generalized rosenzweig-porter random matrix ensemble, *SciPost Physics* **6**, 014 (2019).

[30] G. Biroli and M. Tarzia, Fractal and nonergodic phases in random matrix models, *Phys. Rev. B* **103**, 104205 (2021).

[31] A. V. Lunkin and K. Tikhonov, Local density of states correlations in the Lévy-Rosenzweig-Porter random matrix ensemble, *SciPost Physics* **19**, 015 (2025).

[32] E. Safonova *et al.*, Density of states correlations in Lévy Rosenzweig-Porter model via supersymmetry approach, arXiv preprint (2025), [arXiv:2505.23903](https://arxiv.org/abs/2505.23903).

[33] L. Faoro, M. V. Feigelman, and L. Ioffe, Non-ergodic extended phase of the quantum random energy model, *Ann. Phys.* **409**, 167916 (2019).

[34] V. N. Smelyanskiy *et al.*, Nonergodic delocalized states for efficient population transfer within a narrow band of the energy landscape, *Phys. Rev. X* **10**, 011017 (2020).

[35] M. Winer *et al.*, Spectral form factor of a quantum spin glass, *J. High Energy Phys.* **2022**, 32.

[36] M. Mezard and A. Montanari, *Information, physics, and computation* (Oxford University Press, 2009).

[37] Y. B. Lev *et al.*, Absence of diffusion in an interacting system of spinless fermions on a one-dimensional disordered lattice, *Phys. Rev. Lett.* **114**, 100601 (2015).

[38] K. Agarwal *et al.*, Anomalous diffusion and griffiths effects near the many-body localization transition, *Phys. Rev. Lett.* **114**, 160401 (2015).

[39] N. Macé, F. Alet, and N. Laflorencie, Multifractal scalings across the many-body localization transition, *Phys. Rev. Lett.* **123**, 180601 (2019).

[40] M. Pino *et al.*, Nonergodic metallic and insulating phases of josephson junction chains, *Proc. Natl. Acad. Sci. U.S.A.* **113**, 536 (2016).

[41] M. Pino, V. Kravtsov, B. Altshuler, and L. Ioffe, Multifractal metal in a disordered josephson junctions array, *Physical Review B* **96**, 214205 (2017).

[42] D. M. Long, P. J. D. Crowley, V. Khemani, and A. Chandran, Phenomenology of the prethermal many-body localized regime, *Phys. Rev. Lett.* **131**, 106301 (2023).

[43] M. Tarzia, Many-body localization transition in hilbert space, *Phys. Rev. B* **102**, 014208 (2020).

[44] G. Biroli *et al.*, Large-deviation analysis of rare resonances for the many-body localization transition, *Phys. Rev. B* **110**, 014205 (2024).

[45] T. Thiery *et al.*, Many-body delocalization as a quantum avalanche, *Phys. Rev. Lett.* **121**, 140601 (2018).

[46] W. D. Roeck and F. Huveneers, Stability and instability towards delocalization in many-body localization systems, *Phys. Rev. B* **95**, 155129 (2017).

[47] S. Gopalakrishnan *et al.*, Griffiths effects and slow dynamics in nearly many-body localized systems, *Phys. Rev. B* **93**, 134206 (2016).

[48] E. Altman *et al.*, Quantum simulators: Architectures and opportunities, *PRX Quantum* **2**, 017003 (2021).

[49] M. Schreiber *et al.*, Observation of many-body localization of interacting fermions in a quasirandom optical lattice, *Science* **349**, 842 (2015).

[50] J.-y. Choi, S. Hild, J. Zeiher, P. Schauss, A. Rubio-Abadal, T. Yefsah, V. Khemani, D. Huse, I. Bloch, and C. Gross, Exploring the many-body localization transition in two dimensions, *Science* **352**, 1547 (2016).

- [51] P. Bordia *et al.*, Periodically driving a many-body localized quantum system, *Nature Physics* **13**, 460 (2017).
- [52] T.-M. Li *et al.*, Many-body delocalization with a two-dimensional 70-qubit superconducting quantum simulator, arXiv preprint arXiv:2507.16882 (2025).
- [53] J. Hur *et al.*, Stability of many-body localization in two dimensions, arXiv preprint arXiv:2508.20699 (2025).
- [54] M. Kjaergaard, M. E. Schwartz, J. Braumüller, P. Krantz, J. I.-J. Wang, S. Gustavsson, and W. D. Oliver, Superconducting qubits: Current state of play, *Annual Review of Condensed Matter Physics* **11**, 369 (2020).
- [55] J. P. A. Zúñiga *et al.*, Critical properties of the superfluid - boseglass transition in two dimensions, *Phys. Rev. Lett.* **114**, 155301 (2015).
- [56] L. Leviandier *et al.*, Fourier transform: A tool to measure statistical level properties in very complex spectra, *Phys. Rev. Lett.* **56**, 2449 (1986).
- [57] E. J. Torres-Herrera *et al.*, Generic dynamical features of quenched interacting quantum systems: Survival probability, density imbalance, and out-of-time-ordered correlator, *Phys. Rev. B* **97**, 060303(R) (2018).
- [58] E. J. Torres-Herrera and L. F. Santos, Dynamics at the many-body localization transition, *Phys. Rev. B* **92**, 014208 (2016).
- [59] J. H. Bardarson, F. Pollmann, and J. E. Moore, Unbounded growth of entanglement in models of many-body localization, *Phys. Rev. Lett.* **109**, 017202 (2012).
- [60] Google Quantum AI, Quantum error correction below the surface code threshold, *Nature* **638**, 920 (2025).
- [61] T. I. Andersen, N. Astrakhantsev, A. H. Karamlou, J. Berndtsson, J. Motruk, A. Szasz, J. A. Gross, A. Schuckert, T. Westerhout, Y. Zhang, *et al.*, Thermalization and criticality on an analogue-digital quantum simulator, *Nature* **638**, 79 (2025).
- [62] W. A. Phillips, Two-level states in glasses, *Reports on Progress in Physics* **50**, 1657 (1987).
- [63] L. Faoro and L. B. Ioffe, Internal loss of superconducting resonators induced by interacting two-level systems, *Phys. Rev. Lett.* **109**, 157005 (2012).
- [64] V. K. Varma *et al.*, Energy diffusion in the ergodic phase of a many-body localizable spin chain, *J. Stat. Mech.* , 053101 (2017).
- [65] J. Herbrych and P. Prelovsek, Spin and energy diffusion versus subdiffusion in disordered spin chains, *Phys. Rev. B* **112**, 045108 (2025).
- [66] M. V. Feigel'man, L. B. Ioffe, and M. Mézard, Superconductor-insulator transition and energy localization, *Phys. Rev. B* **82**, 184534 (2010).
- [67] R. Abou-Chakra, D. J. Thouless, and P. W. Anderson, A self-consistent theory of localization, *J. Phys. C* **6**, 1734 (1973).
- [68] V. E. Kravtsov, B. L. Altshuler, and L. B. Ioffe, Non-ergodic extended states in disordered systems, *Ann. Phys.* **389**, 148 (2018).
- [69] B. Derrida and H. Spohn, *Journal of Statistical Physics* **51**, 817 (1988).
- [70] B. Derrida, *Physica A* **163**, 71 (1990).
- [71] G. Biroli, G. Semerjian, and M. Tarzia, *Progress of Theoretical Physics Supplement* **184**, 187 (2010).

## CONTENTS

References	7
1. List of symbols	11
2. Experimental details	12
2.A. Procedure	12
2.B. Data fitting	12
3. Qualitative theoretical description	13
3.A. Short time dynamics of return probability	13
3.B. $1/f$ spin noise	13
3.C. Exponent $\eta$ and its $n$ -dependence.	14
3.D. Dephasing without relaxation: results of a model calculation	15
4. Recursion relations for spin- $\frac{1}{2}$ model on the Cayley tree	16
4.A. Preliminaries	16
4.B. Recursion equations for the relaxation rates	17
4.C. Calculation of dephasing rates	17
a. Schrieffer - Wolff transformation	17
b. Recursion equations for dephasing	18
5. Thresholds for the relaxation and dephasing channels	19
5.A. “Upper limit” approximation	19
a. Relaxation rate	19
b. Dephasing rate	19
5.B. Account for self-energy correction	20
a. Relaxation rate threshold	20
b. Dephasing rate threshold	20

## 1. LIST OF SYMBOLS

Symbol	Description
$J$	Spin-spin coupling strength (XY interaction)
$H$	Hamiltonian of the spin- $\frac{1}{2}$ model on the Cayley tree
$\sigma_i^a$	Pauli matrices (where $a = x, y, z$ or $1, 2, 3$ ), $\sigma_i^a = 2S_i^a$
$\sigma_i^\pm$	Raising and lowering spin operators, $S_i^\pm$
$h_i$	Random magnetic field at site $i$
$W$	Full width of the box distribution for $h_i$
$n$	Total number of spins (or system size)
$K$	Branching number of the Cayley tree (CT)
$Z$	Full coordination number of sites on CT, $Z = K + 1$
$\mathcal{H}$	Operator $\hat{1} \otimes H^T - H \otimes \hat{1}$ in the extended Hilbert space
$ \hat{O}\rangle$	Operator $\hat{O}$ represented as a wave function in the extended space
$\mathcal{V}$	Perturbation operator in the extended space, related to $V$
$\Gamma_i^r, \Gamma_j^\pm$	Local relaxation rate for spin at site $i$ (or $j$ )
$\Sigma_z(\epsilon)$	Self-energy for the $z$ -component of spin operator
$\Sigma_\pm(\epsilon)$	Self-energy for the $\sigma^\pm$ components
$U$	Anti-hermitian operator for Schrieffer - Wolff transformation
$H_{eff}$	Effective Hamiltonian after Schrieffer - Wolff transformation
$V_{eff}$	Effective perturbation Hamiltonian, $\frac{1}{2}[V, U]$
$\Gamma_j^\phi$	Local dephasing rate for spin at site $j$
$J_r, j_r$	Critical coupling strength and dimensionless ratio ( $j_r = J_r/W$ ) for relaxation
$J_\phi, j_c$	Critical coupling strength and dimensionless ratio ( $j_c = J_\phi/W$ ) for dephasing
$F(x)$	Function used to determine the critical point of linear recursions
$P_0(h)$	Bare distribution function for the local field $h$
$P_1(h)$	Effective distribution function for $h$ accounting for self-energy correction (relaxation)
$P_2(h_1, h_2)$	Renormalized distribution function for $h_1, h_2$ (dephasing)
$G(e^{-x})$	Laplace transform of the probability density function $\mathcal{P}(\Gamma_j)$
$S$	$\text{Re } \Sigma$ , the real part of the self-energy correction (dephasing)

## 2. EXPERIMENTAL DETAILS

### 2.A. Procedure

The experiments were performed on a Willow device architecture as presented in Ref. [60], using the calibration protocols shown in Ref. [61] to set the coupling rates and  $Z$ -fields of the analog Hamiltonian. Since the Hamiltonian is photon number conserving, we mitigate the effects of photon loss by postselecting the data, removing any bitstrings in which the photon number is not conserved.

In all experiments, the qubit frequencies are first ramped quickly ( $\sim 1$  ns) to the values corresponding to the relevant disorder instance, before ramping up the coupling rates over another  $\sim 1$  ns. The system is then evolved for a variable amount of time under the analog Hamiltonian, followed by a 1 ns Hamiltonian off-ramp, and finally measurements in the  $Z$ -basis.

### 2.B. Data fitting

As discussed in the main text, the dependence of Edwards-Anderson order parameter on time fits well the power law,  $C_{fit}(t) = at^{-\alpha}$  at low  $w < w_c \approx 10$  and fits well exponential law at  $w > w_c$  with non-zero offset:  $C_{fit}(t) = a \exp(-\Gamma't) + Q_{EA}$  or  $C_{fit}(t) = at^{-\alpha} \exp(-\Gamma't) + Q_{EA}$  close to the transition. This statement can be made more quantitative if we compare the actual data with the fits and define quality of fit,  $\chi$  by

$$\chi = \frac{1}{n_t} \sum_t \left( \frac{C_{fit}(t) - C_t}{C_t} \right)^2 \quad (S6)$$

where  $n_t$  is the number of data points in time,  $C_{fit}(t)$  is the fitting function and  $C_t$  is filtered value of measured magnetization squared after time  $t$ ,  $m_t^2 = (1/n) \sum_i \langle \sigma_i^z(t) \rangle^2$ . The measured values of  $m_t^2$  fluctuates significantly over time, even after being averaged over 100 realizations. These fluctuations dominate the fit quality  $\chi$  at large disorders, to prevent this we smoothed the data by applying Savitsky Golay filter,  $G_r$  with degree  $r = 2 - 5$  to the data:  $C_t = \sum_t G_r(t-t')m_t^2$ . We emphasize that the fit parameters are not affected by the application of the filter, it affects only the evaluation of the fit quality,  $\chi$ . Slightly above the transition the best fit is achieved by exponential with the power law prefactor and offset, see Fig.S5a that illustrates the typical behavior in this regime. Below the transition, at  $w < w_c \sim 10$  the power law fit is very good but fails above it, see Fig.S5b. Similarly exponential fits with offset are not good below transition but become very good above it. Far above the transition, exponential and exponential with power law prefactor and offsets are equally good, in this regime the exponent  $\alpha$  of the power law becomes very small, e.g.  $\alpha = 0.15$  for  $w = 20$ , which makes it very difficult to distinguish the fits. In this regime, the values of the offset for these two fits are practically identical.

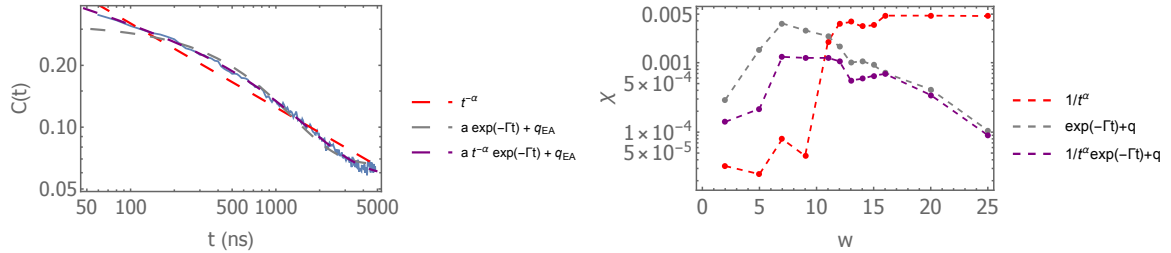


**FIG. S5:** Comparison of remanent magnetization fits by different time dependencies. Left panel: data for  $n = 59$   $w = 14$  and their fits with different laws, with and without offset. The data shown here were filtered with degree  $r = 2$  filter. Right panel: data deviation from different fits as a function of  $w$  for  $n = 59$ . Below phase transition power law is clearly a winner, while above the transition exponential fit with offset quickly wins over the power law. One cannot distinguish pure exponential and exponential with a power law prefactor.

### 3. QUALITATIVE THEORETICAL DESCRIPTION

#### 3.A. Short time dynamics of return probability

Short time behavior of  $R(t)$  at  $Jt \leq 1$  is well-described by the simplest approximation of independent spin pairs defined by the Hamiltonian:

$$H_0 = \sum_{\mu} H_{\mu} = \sum_{\mu} [J\tau_{\mu}^x + \varepsilon_{\mu}\tau_{\mu}^z] \quad (\text{S7})$$

where  $\tau_{\mu}$  denote Pauli matrices of combined spin operators on the links:  $\tau_{\mu}^x = S_r^+ S_{r'}^- + h.c.$ ,  $\tau_{\mu}^z = S_r^z - S_{r'}^z$ , while  $\mu \equiv \langle r, r' \rangle$  are defined on each lattice bond and  $\varepsilon_{\mu} \equiv \varepsilon_{r,r'} = \frac{1}{2}(h_r - h_r')$ . The meaning of approximation (S7) is to account for spin-flip events that occur at each link  $\mu$  in the lowest order over coupling  $J$ ; here we mean, in terms of original spins  $\mathbf{S}_r$ , a projection of the two-spin Hilbert space (dimension 4) to the subspace  $|\uparrow\downarrow\rangle, |\downarrow\uparrow\rangle$  only. It works fine for  $Jt \leq 1$  as one can observe comparing the corresponding data in Fig. S6 with the calculation based on the Hamiltonian (S7), see below. The result of such calculation reads as follows:

$$\prod_{\langle r, r' \rangle} \left[ 1 - \frac{J^2}{\varepsilon_{r,r'}^2 + J^2} \sin^2 \left( t \sqrt{\varepsilon_{r,r'}^2 + J^2} \right) \right] \quad (\text{S8})$$

where product goes over all  $2n$  pairs of nearest neighbors. Each multiplier in the R.H.S. of Eq.(S8) describes the independent dynamics of "effective spins"  $\tau_{\mu}$  defined on each lattice bond  $\langle r, r' \rangle \equiv \mu$  and governed by the sum of local Hamiltonians (S7).  $R(t)$  defined by Eq.(S8) is a random quantity that depends on specific realization of  $h_r$ . Representative  $R(t)$  can be obtained by the averaging of  $\ln R(t)$  over  $h_r$ , since this is an additive quantity:  $R_{typ}(t) = \exp\{\overline{\ln R(t)}\}$ , where  $\overline{[...]} \equiv \overline{[...]}_{h_r}$  denotes averaging over independent random  $h_r$ . Approximation of independent pairs (S8) leads to a finite disorder-dependent limit for  $R_{typ}(\infty)$  that can be calculated as

$$-\ln R_{typ}(\infty) \approx 2n \frac{4(\pi - 2)}{w} \quad (\text{S9})$$

Factor  $2n$  comes from the number of bonds on square lattice of  $n$  sites, the integral over distribution of  $\varepsilon_{r,r'}$  is calculated in the leading approximation over  $1/w \ll 1$ .

Numerically evaluated expression for  $R_{typ}(t)$  computed for  $w = 15$  with the help of (S8) is shown in Fig. S6a by blue dashed line (for  $n = 25$ ) and grey dashed line,  $n = 36$ . Results of direct numerical simulation of  $R_{typ}(t)$  for  $n = 16, 20$  and two instances of  $n = 25$  are shown by full lines, together with experimental data for  $n = 36$ . Good agreement between approximation (S8) and the data is seen till  $Jt \approx 1$  corresponding to  $t \approx 30$ ns, while at later time-scales qualitative deviations occur. Indeed, while theoretical dashed curves shows damped oscillations approaching constant value at  $t \rightarrow \infty$ , the data (in red) demonstrate faster decay of the oscillation amplitude and overall downshift of  $R(t)$ , in agreement with Eq.(2) of the Main text. We will argue below that such a behavior is due to residual interaction between different spin pairs  $\tau_{\mu}, \tau_{\nu}$  leading to dephasing and inelastic transitions.

Power-law behavior at long times [Eq.(2) of the Main text] means that probability for a flip of any spin  $S_r$  of the array grows logarithmically with time like  $P_{\text{flip}} \sim (\eta/n) \ln(Jt)$ ; such a behavior is akin to spin noise with  $1/f$  power spectrum, known to be generic for glasses and spin glasses. Indeed, numerical simulations (see next Subsection) demonstrate spin noise spectrum  $\mathcal{S}(\omega) = \langle |S^z(\omega)|^2 \rangle \approx \frac{A}{|\omega|}$ .

#### 3.B. $1/f$ spin noise

Slow relaxation in glasses or spin glasses is usually associated with the presence of a broad spectrum  $P(\Gamma)d\Gamma$  of relaxation rates  $\Gamma$  which characterize dynamics of various modes of fluctuations, frequently considered as two-level systems. Once the assumption of a broad distribution  $P(\Gamma)d\Gamma \sim d\Gamma/\Gamma$  is made, it leads immediately [18] to the prediction of the noise spectrum  $\mathcal{S}(\omega) \propto 1/|\omega|$ . To check if such a noise is present in our system, we implement numerical simulation of its dynamics for the system size  $n = 20$ . We compute local spin-spin correlation function  $S_r(t) = \langle S_r^z(0)S_r^z(t) \rangle$  and then average over positions  $\mathbf{r}$  and realizations of disorder, to obtain  $S(t) = \langle S_r^z(0)S_r^z(t) \rangle$ . Its Fourier transform  $\mathcal{S}(\omega)$  is plotted in Fig. S6b and features  $1/f$  noise over two decades in frequency.

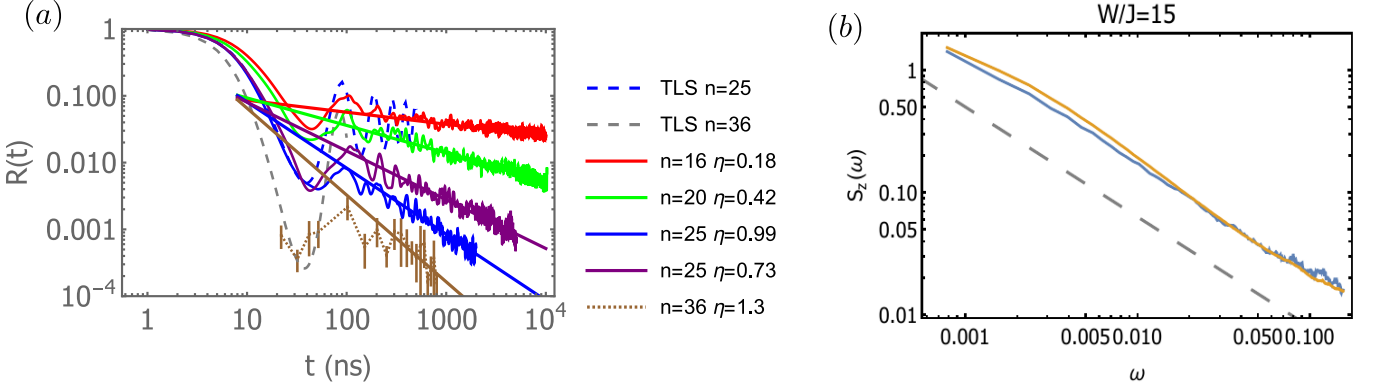


**FIG. S6:** Panel a): Return probability  $R(t)$  for moderate disorder  $w = 15$ ; dashed lines obtained with model Hamiltonian (S7), full lines numerically for  $n = 16, 20, 25$ , dotted line is for experimental data for  $n = 36$ . Panel b): Power spectrum of local spin  $S^z(t)$  fluctuations: numerical simulation on the system of  $n = 20$  spins with  $w = 15$ .

### 3.C. Exponent $\eta$ and its $n$ -dependence.

To explain power-law decay of  $R(t)$  with exponent  $\eta \propto n^2$ , we refer to phenomenology of two-level systems in glasses [62] and to the related mechanism of  $1/f$  noise [18]. The key point is the existence of a broad spectrum of very low frequencies in a system. Hamiltonian (S7) is not sufficient in that respect, since all its eigenvalues are  $\geq J$ . Thus it is natural to take into account the interactions between effective spins  $\tau_\mu$  which makes possible correlated flips of the pairs of them, with small change of the total energy of a pair, see e.g. [63? ]. Beforehand notice that the dependence (3)[Main text] cannot be valid at arbitrary large  $n \rightarrow \infty$  since at any fixed large  $Jt$  it would make  $R(t)$  smaller than the minimal IPR value  $I_2^{\min} = 2^{-n}$ . However, due to smallness of  $\kappa(w) \leq 1/w^2$ , [see Eq.(5) of the Main text], the upper bound  $n_{\max} \geq w^2$  compatible with such a dependence exceeds the maximal size of our system, even for the critical disorder  $w \approx w_r$ . Thus our results for  $\eta(n)$  dependence refer to the intermediate asymptotics of *moderately large* systems with  $1 \ll n \leq n_{\max}(w)$ . It will be sufficient to consider small fraction  $\sim 2/w \ll 1$  of all effective spins which have  $\epsilon_\mu \leq J$  - we will call them "coherent TLS". Interaction Hamiltonian is then

$$H_{\text{int}} = \frac{1}{2} \sum_{\mu\nu} V_{\mu,\nu} (\tau_\mu^+ \tau_\nu^- + h.c.) \quad (\text{S10})$$

so that the full Hamiltonian consists of Eqs.(S7,S10). Total number of effective spins is about  $n_* = 4n/w \gg 1$ . Matrix elements  $V_{\mu,\nu}$  appear in higher orders of perturbation theory over  $j = 1/w \ll 1$ : these are interactions between rare active TLS via "inert media" of all other spins. Therefore  $V_{\mu,\nu}$  are mostly small compared to  $J$ , and statistical distribution of their absolute values is very broad. Writing  $|V_{\mu,\nu}| = J \exp(-L_{\mu,\nu})$  we present this distribution via

$$\mathcal{P}(L) dL \approx P_1 dL \quad \text{where} \quad L_{\min} < L < L_{\max} \quad (\text{S11})$$

with  $L_{\min} \sim \ln w$  and  $L_{\max} \sim n_* \ln w \gg L_{\min}$ .

Now we formulate the key assumption of the further theoretical analysis: the system of interacting TLS's is characterized (in the range  $w$  corresponding to the glassy state) by dephasing rate  $\Gamma_\phi$  that is much larger than relaxation rate  $\Gamma$ . Theoretical arguments demonstrating possibility of such a situation are provided below in Secs. 4 and 5 below. Qualitatively, spin dephasing without spin relaxation is equivalent to the presence of energy transport in the absence of full ergodicity; usual low-temperature glasses provide useful example of such a situation. Indeed, dephasing-only is present as soon as effective magnetic field  $h_r^z$  acting in a site  $r$ , appears to be slowly-time-dependent due to coupling of  $\mathbf{S}_r$  with other spins; since full energy of the system is conserved, it is possible if energy transport is allowed between different parts of the system. Within MBL framework, studies of energy transport were provided in Ref. [64, 65].

We expect  $\Gamma_\phi \ll J$  but still larger than most of the matrix elements  $V_{\mu,\nu}$  since the latter are due to high-order processes. Then *real transitions* leading both to  $1/f$  noise and to logarithmic growth of  $-\ln R(t)$  occur due to interaction (S10) between pairs of active TLS with small  $|E_\mu - E_\nu|$ , where  $E_\mu = \sqrt{\epsilon_\mu^2 + J^2}$ . Estimate for the rate  $r_{\mu\nu}$  of such (incoherent) transition is given by  $r_{\mu\nu} \sim V_{\mu,\nu}^2 \Gamma_\phi / |E_\mu - E_\nu|^2$  (compare with Eq.(26) from Ref. [18]). Exponentially broad distribution of matrix elements  $V_{\mu,\nu}$  defined by Eq.(S11) translates then to the same kind of

distribution for the rates  $r_{\mu\nu} \sim \Gamma_\phi e^{-2L_{\mu\nu}}$ . Factor  $P_1$  in Eq.(S11) is proportional to  $n$  due to the normalization condition  $\int \mathcal{P}(L)dL = P_1 L_{\max} \propto n_*^2$  since total number of pairs of interacting TLS scales as  $n_*^2$ , and also  $L_{\max} \propto n_*$ . In result, we find that  $P_1 = \gamma n$  where  $\gamma \equiv \gamma(w)$ .

Probability for any spin to be involved in inelastic relaxation during long time  $t \gg 1/J$  grows  $\propto \gamma n \ln(Jt)$ . Now, in order to obtain the estimate for the full probability of return  $R(t)$ , one needs to take into account that  $\ln R(t)$  is additive over all spins, thus an additional multiplication on the number of spins  $n$  should be performed. This way one gets power-law decay,  $R_{\text{typ}}(t) \sim (Jt)^{-\eta}$ , with exponent  $\eta \propto n^2$ , not far from its experimentally observed dependence in Eq.(3) of the Main text.

### 3.D. Dephasing without relaxation: results of a model calculation

Our analysis provided above that explains power-law dependence  $R(t) \sim 1/t^\eta$  with  $\eta(n) \propto n^2$ , is based on the assumption of dephasing rate  $\Gamma^\phi$  being much higher than rate of inelastic relaxation  $\Gamma^r$ . In fact, we assumed that non-zero  $\Gamma^\phi > 0$  is generated at  $j_c < J/W \ll 1$  once original couplings  $J$  between neighboring spins in the Hamiltonian (1) [Main text] are taken into account, while for relaxation (real spin flips) an analogous critical value  $j_r = J_r/W$  is larger,  $j_r > j_c$ . In such a case at  $j_c < J/W < j_r$  relaxation processes are due to high-order terms of the  $J/W$  expansion, thus the inequality  $\Gamma^r \ll \Gamma^\phi$  holds. Below in Sec.4 we present a calculation for the Hamiltonian (1) of the Main text, but living on the Cayley tree with branching number  $K \gg 1$ , which demonstrates  $j_c \ll j_r$ . Here in this Subsection we provide a brief account of that calculation, concentrating on its main results.

We define  $\Gamma^\phi$  as  $\text{Im } \Sigma^\pm$  where  $\Sigma^\pm(\omega)$  is the self-energy part corresponding to transverse spin Green function  $G^\pm(\omega)$ ; similarly, relaxation rate  $\Gamma^r$  is defined via self-energy of longitudinal Green function  $G^{zz}(\omega)$ . Using Heisenberg equations for spin operators and using the absence of loops on Cayley tree, one can derive (see next Sec.4) recursion relations for local relaxation rates  $\Gamma_i^r$ , similar (but different) to those of Ref.[66]:

$$\Gamma_0^r = J^2 \sum_j \frac{\Gamma_j^r}{(h_j - h_0)^2} \quad (\text{S12})$$

Summation here goes over  $K$  neighbors of the "central spin"  $\mathbf{S}_0$ . Below we use bare distribution of local energies  $P_0(h) = \frac{1}{W} \theta(W/2 - |h|)$ . Recursions (S12) converge under iterations to  $\Gamma^r = 0$  at  $J < J_r$  while at larger  $J$  linear iterations diverge and nonlinear in  $\Gamma^r$  terms are needed to get a final nonzero result. Next, we assume  $J < J_r$  and derive (in the next order over  $J^2$ ) analogous equations for  $\Gamma^\phi$ :

$$\Gamma_0^\phi = J^4 \sum_{j \neq k} \left( \frac{1}{h_0 - h_j} + \frac{1}{h_0 - h_k} \right)^2 \frac{\Gamma_j^\phi + \Gamma_k^\phi}{(h_j - h_k)^2} \quad (\text{S13})$$

Summation goes over  $K(K-1)/2$  pairs of unequal neighbors of the site 0. Eqs.(S13) can be used to determine the boundary of the parameter region where non-zero  $\Gamma^\phi$  are generated, that is  $J_c = J_c(K)$ . In general, equations for  $\Gamma^\phi$  contain also terms of order  $J^2$ , but these terms are inefficient at  $J < J_r$  and thus omitted here.

At very small  $J/W$  we can neglect correlations between  $\Gamma_i^r$  at some site  $i$  and local field  $h_i$ ; it amounts to setting  $h_0 = 0$  in Eq.(S12). Then these equations become identical to those derived in Ref. [67] for Anderson localization on a tree (of branching number  $K$ ), within simplest "upper limit" approximation that neglects level repulsion (that is, real part of self-energy). Then critical value  $j_r = J_r/W$  obeys simple equation  $(2j_r)^{-1} = eK|\ln(2j_r)|$ . Its solution for  $K = 3$  is  $j_r \approx 1.86 \cdot 10^{-2}$ . Generalizing the same procedure for recursion equations (S13), one can find (see Sec. 5 below) the critical value  $j_c = J_c/W$  within "upper limit approximation" equal to  $j_c = 1.5 \cdot 10^{-2}$ , thus confirming that  $j_c < j_r$ . The same inequality survives for larger values of  $K$ .

One can make a better calculation for both  $j_r$  and  $j_c$  taking into account corrections to the real part of self-energy function. For Eq.(S12) we can follow closely the approach proposed in Ref. [68] and get  $j_r = 0.03$  for  $K = 3$ . Generalization of the same approach to the case of recursions (S13) is provided in Sec.5 below and leads to  $j_c = 0.02$  at  $K = 3$ . The ratio  $j_r/j_c \approx 1.5$  was found for larger values of  $K$  as well. We conclude that various approximation schemes consistently support our qualitative picture: in some range of  $W$  values the single-spin dephasing rate is much stronger than its relaxation rate.

#### 4. RECURSION RELATIONS FOR SPIN- $\frac{1}{2}$ MODEL ON THE CAYLEY TREE

The main goal of the theory developed below is to demonstrate that local nature of spin-spin interaction in a random system may lead to the situation when local spin dephasing time is typically much shorter than spin relaxation time. To show it, as a matter of principle, we will use drastic simplification of our problem; namely, we consider spins  $\frac{1}{2}$  siting on a Cayley tree (infinite Bethe lattice) instead of a real square lattice.

##### 4.A. Preliminaries

We are going to study a system of spins- $\frac{1}{2}$  in a random magnetic field with XY interaction on a Cayley tree (CT) with large branching number  $K \gg 1$ . The Hamiltonian is of the following form:

$$H = -J \sum_{\langle i,j \rangle} (\sigma_i^+ \sigma_j^- + \sigma_j^+ \sigma_i^-) + \frac{1}{2} \sum_i h_i \sigma_i^z. \quad (\text{S14})$$

where  $i, j$  are sites the Cayley tree, summation in the first term goes over links  $\langle i, j \rangle$  of nearest neighbours. Random variables  $h_i$  belong to uncorrelated symmetric box distribution of full width  $W$ . Operators  $\sigma_i^a = 2S_i^a$  with  $a = 1, 2, 3$  are Pauli matrices, while  $\sigma_i^\pm \equiv S_i^\pm$ . Thus Hamiltonian (S14) is equivalent to the Hamiltonian (1) from the Main text up to the replacement of square lattice by the Cayley tree. Full coordination number of sites of CT is  $Z = K + 1$  and we have in mind correspondence to original square lattice, so the "most realistic" value of branching number is  $K = 3$ .

Our main goal is to derive, using loopless structure of the Cayley tree, a kind of recursion relations between i) local relaxation rates  $\Gamma_i^r$  for spins which belong to different sites  $i$  of the CT, and ii) local dephasing rates  $\Gamma_i^\phi$  for the same spins. To realize this program, it will be useful to represent Heisenberg equations for spin operators in the form similar to Schrodinger equations for wavefunctions. The advantage of this approach is that it keeps track of local nature of interactions in the Hamiltonian (S14), which is somewhat hidden in many-body wavefunctions.

The evolution equation for the operators is a linear equation and to rewrite it as a Schrödinger-type equation we introduce the mixed state of our system with its copy:

$$|\hat{1}\rangle := \bigotimes_j \left[ \frac{|00\rangle_j + |11\rangle_j}{\sqrt{2}} \right] = \frac{1}{\sqrt{2^n}} \sum_s |s\rangle \otimes |s\rangle \quad (\text{S15})$$

where  $n$  is the total number of spins. In the last terms sum runs over all bit-strings. Using this mixed state we can consider each operator as a wave function in the extended Hilbert space (of original system and its copy):

$$|\hat{O}\rangle = \hat{O} \otimes \hat{1} |\hat{1}\rangle \quad (\text{S16})$$

We note the following useful property:  $\hat{O} \otimes \hat{1} |\hat{1}\rangle = \hat{1} \otimes \hat{O}^T |\hat{1}\rangle$ . The evolution equation acquires then the following form:

$$\begin{aligned} i\partial_t |\hat{O}(t)\rangle &= \mathcal{H} |\hat{O}(t)\rangle \equiv |[\hat{O}(t), H]\rangle \quad \text{where} \\ \mathcal{H} &= \hat{1} \otimes H^T - H \otimes \hat{1} \end{aligned} \quad (\text{S17})$$

Below we consider Hamiltonian (S14) as a sum  $H = H_0 + V$  where "bare Hamiltonian"  $H_0$  coincides with the second sum in (S14) while "perturbation"  $V$  is given by the first term. The states  $|\sigma_j^z\rangle$ ,  $\sqrt{2}|\sigma_j^\pm\rangle$  (in the extended Hilbert space) are normalized eigenstates of  $\mathcal{H}_0$  with eigenvalues 0 and  $\pm h_j$  respectively.

The action of the perturbation  $\mathcal{V}$  on the operators  $\sigma_j^z$  and  $\sigma_j^\pm$  is as follows:

$$\begin{aligned} \mathcal{V} |\sigma_j^z\rangle &= J \sum_{k \in \partial j} |[\sigma_j^z, \sigma_j^+ \sigma_k^- + \sigma_j^- \sigma_k^+]\rangle \\ &= 2J \sum_{k \in \partial j} (|\sigma_j^+ \sigma_k^-\rangle - |\sigma_j^- \sigma_k^+\rangle) \end{aligned} \quad (\text{S18})$$

and

$$\mathcal{V}|\sigma_j^\pm\rangle = \pm J \sum_{k \in \partial j} |\sigma_j^z \sigma_k^\pm\rangle \quad (\text{S19})$$

Here  $k \in \partial j$  means that  $k$  is a neighbor of  $j$ .

Now we calculate relaxation rate  $\Gamma^\pm$  in this spin model. The relaxation rate is given by the imaginary part of the self-energy  $\Sigma_z$  which reads:

$$\Sigma_z(\epsilon) = \text{Im}\langle \sigma_j^z | \mathcal{V}(\epsilon - \mathcal{H} + i0)^{-1} \mathcal{V} | \sigma_j^z \rangle \quad (\text{S20})$$

Now we use approximation of high connectivity,  $K \gg 1$ . It allows us to consider dynamics of neighboring spins being weakly correlated, thus  $\langle \sigma_j^+(t) \sigma_k^+(t) | \sigma_j^+ \sigma_k^+ \rangle \approx \langle \sigma_j^+(t) | \sigma_j^+ \rangle \langle \sigma_k^+(t) | \sigma_k^+ \rangle$ . This is a kind of self-consistent born approximation, like the one used in Ref. [1]. The resulting self-energy for  $z$ -component of spin is given by:

$$\begin{aligned} \Sigma_z^{(j)}(\epsilon) = 2J^2 \sum_{k \in \partial} & [\langle \sigma_k^- | (\epsilon - h_j - \mathcal{H} + i0)^{-1} | \sigma_k^- \rangle + \\ & \langle \sigma_k^+ | (\epsilon + h_j - \mathcal{H} + i0)^{-1} | \sigma_k^+ \rangle] \end{aligned} \quad (\text{S21})$$

In the same way, self-energy for  $\sigma^\pm$  components can be found in the form

$$\Sigma_\pm^{(j)}(\epsilon) = 2J^2 \sum_{k \in \partial j} \langle \sigma_k^\pm | (\epsilon - \mathcal{H} + i0)^{-1} | \sigma_k^\pm \rangle \quad (\text{S22})$$

#### 4.B. Recursion equations for the relaxation rates

Relaxation rate  $\Gamma_j$  can be found either via the imaginary part of  $\Sigma_z^{(j)}(\epsilon)$  at very low energy  $\epsilon \rightarrow 0$  or via the imaginary part of  $\Sigma_\pm^{(j)}(\epsilon)$  at  $\epsilon = h_j$ . Calculations of  $\text{Im} \Sigma$  using Eq.(S21) in the first case, or Eq.(S22) in the second case, lead to identical results, so we obtain the following self-consistent equation for  $\Gamma_j^\pm$ :

$$\Gamma_j^\pm = J^2 \sum_{k \in \partial j} \frac{\Gamma_k^\pm}{(h_j - h_k)^2 + (\Gamma_k^\pm)^2} \quad (\text{S23})$$

Summation in Eq.(S23) goes over  $K$  descendants of the site  $j$ . Below in Sec. 5 we will find critical magnitude of  $J_r = j_r W$  such that at  $J > J_r$  recursions (S23) lead to nonzero relaxation rates  $\Gamma_j^\pm$ .

#### 4.C. Calculation of dephasing rates

##### a. Schrieffer - Wolff transformation

Now suppose we consider range of couplings  $J < J_r$  where lowest-order perturbation theory over  $J/W$  does not lead to relaxation and dephasing; in other terms, recursion relations (S23) leads to trivial solution with vanishing  $\Gamma^\pm$ . We are going to show that in fact this result does not mean that dephasing is really absent in our system. To demonstrate it, we study second-order processes, which may lead to *pure dephasing* without relaxation.

It is convenient to employ Schrieffer - Wolff unitary transformation generated by anti-hermitian operator  $U$ .

Then the effective Hamiltonian becomes of the form

$$H_{\text{eff}} = H + [H, U] + \frac{1}{2}[[H, U], U] + \dots \quad (\text{S24})$$

We are going to find operator  $U$  such that  $H_{\text{eff}}$  will not contain terms which are linear in  $J$  and proportional to  $\sigma_j^\pm$ . Let  $U = \sum_{\langle j, k \rangle} s_{jk} (\sigma_j^+ \sigma_k^- - \sigma_j^- \sigma_k^+)$ . Then we need to obey

$$[H_0, U] + V = 0. \quad (\text{S25})$$

The above equation gives:  $s_{jk} = J/(h_j - h_k)$ . Then the effective Hamiltonian is  $H_{eff} = H_0 + V_{eff}$  where  $V_{eff} = \frac{1}{2}[V, U]$ . Calculating the commutator, we find

$$V_{eff} = \frac{J}{2} \sum_{\langle j, k \rangle} \sum_{\langle l, m \rangle} s_{jk} [\sigma_l^+ \sigma_m^- + \sigma_l^+ \sigma_m^-, \sigma_j^+ \sigma_k^- - \sigma_k^+ \sigma_j^-] \quad (\text{S26})$$

The commutator in Eq.(S26) is not vanishing if the edges  $(j, k)$  and  $(l, m)$  coincide or have at least one common vertex. Thus we can rewrite  $V_{eff}$  as follows:

$$V_{eff} = \frac{J}{2} \sum_{\langle j, k \rangle} s_{jk} (\sigma_k^z - \sigma_j^z) - \frac{J}{2} \sum_j \sum_{(l, k) \in \partial j} (s_{jk} + s_{lj}) \sigma_j^z (\sigma_l^+ \sigma_k^- + \sigma_l^- \sigma_k^+) \quad (\text{S27})$$

Here sign  $(l, k) \in \partial j$  means that the sum runs over all possible pairs of neighbors of  $j$ -th vertex. Effective perturbation Hamiltonian (S27) will be used below to calculate dephasing rates.

### b. Recursion equations for dephasing

We will use the formalism of the previous Subsection to find a dephasing rate, with a focus on dynamics of operator  $\sigma_j^+$ . The action of the perturbation  $V_{eff}$  on a  $\sigma_j^+$  can be written, in the extended space, in the form

$$\mathcal{V}_{eff} |\sigma_j^+ \rangle \approx \sum_{(m, k) \in \partial j} (s_{jk} + s_{mj}) |\sigma_j^+ (\sigma_k^+ \sigma_m^- + \sigma_k^- \sigma_m^+) \rangle \quad (\text{S28})$$

Note, that we take into account the terms proportional to  $\sigma_j^z$  only, while other terms which are usually responsible for decay process are neglected; the reason is our assumption that  $J/W$  is too small to generate decay self-consistently.

The corresponding self-energy is:

$$\begin{aligned} \Sigma_j^+(\epsilon) &= 4J^2 \sum_{(m, k) \in \partial j} (s_{jk} + s_{jm})^2 \langle \sigma_k^+ \sigma_m^- | (\epsilon - h_j - \mathcal{H}_{eff} + i0)^{-1} | \sigma_k^+ \sigma_m^- \rangle \approx \\ &4J^2 \sum_{(m, k) \in \partial j} (s_{jk}^2 + s_{jm}^2) \langle \sigma_k^+ \sigma_m^- | (\epsilon - h_j - \mathcal{H}_{eff} + i0)^{-1} | \sigma_k^+ \sigma_m^- \rangle \end{aligned} \quad (\text{S29})$$

The dephasing rate  $\Gamma^\phi$  is given by the imaginary part of the self-energy  $\text{Im } \Sigma_j^+(\epsilon)$  at  $\epsilon = h_j$ . To estimate a correlation function of the operator  $\sigma_k^+ \sigma_m^-$  we use large connectivity limit  $K \gg 1$  and suppose that this correlation function is factorized in the time domain, due to weak correlations between different spins; the same approximation was used in the previous Section while deriving Eq.(S21,S22). The resulting equation for the self-energy reads as follows:

$$\begin{aligned} \Sigma_j^+(h_j + \delta\epsilon) &= 4J^2 \sum_{(m, k) \in \partial j} (s_{jk}^2 + s_{jm}^2) i \int \frac{d\epsilon_1}{2\pi} \langle \sigma_k^+ | (\epsilon_1 - \mathcal{H}_{eff} + i0)^{-1} | \sigma_k^+ \rangle \times \\ &\langle \sigma_m^- | (\delta\epsilon - \epsilon_1 - \mathcal{H}_{eff} + i0)^{-1} | \sigma_m^- \rangle \approx J^2 \sum_{(m, k) \in \partial j} \frac{s_{jk}^2 + s_{jm}^2}{h_m - h_k + i(\Gamma_k^\phi + \Gamma_m^\phi)} \end{aligned} \quad (\text{S30})$$

Calculating the imaginary part of the above self-energy we find the (linearized form of) recursion equation for the dephasing rate:

$$\Gamma_j^\phi = J^4 \sum_{(m, k) \in \partial j} \left( \frac{1}{(h_j - h_k)^2} + \frac{1}{(h_j - h_m)^2} \right) \frac{\Gamma_k^\phi + \Gamma_m^\phi}{(h_k - h_m)^2} \quad (\text{S31})$$

Recursion equation (S31) will be used below in Sec.5 for determination of the threshold value  $j_c = J_c/W$  for the existence of self-consistent dephasing in our spin system.

## 5. THRESHOLDS FOR THE RELAXATION AND DEPHASING CHANNELS

### 5.A. “Upper limit” approximation

#### a. Relaxation rate

At very small  $J/W$  we can neglect correlations between  $\Gamma_i^r$  at some site  $i$  and local field  $h_i$ ; it amounts to setting  $h_0 = 0$  in Eq.(S23). Then these equations become identical to those derived in Ref. [67] for Anderson localization on a tree (of branching number  $K$ ), within simplest “upper limit” approximation that neglects level repulsion (in other terms, real part of self-energy is neglected). The critical value  $j_r = J_r/W$  can be found from the analysis of the linearized version of Eq.(S23). Instability point of this linear recursion (with  $\Gamma^\pm$  neglected in denominator in R.H.S.) is determined by the set of two equations

$$\frac{dF}{dx} |_{x=x_*} = 0; \quad F(x_*) = 0 \quad (\text{S32})$$

where  $F(x) \rightarrow F_1(x)$  and

$$F_1(x) = \frac{1}{x} \ln \left\{ K \int P_0(h) dh [J^2 \cdot f(h)]^x \right\} \quad (\text{S33})$$

where  $P_0(h) = (1/W)\theta(\frac{W}{2} - |h|)$ . Equations (S32,S33) can be derived using theory of freezing transition for random polymers on a tree [69, 70]. Solving the above set of equations one finds algebraic equation

$$\frac{1}{2j_r} = eK \ln \frac{1}{2j_r} \quad (\text{S34})$$

Its solution for  $K = 3$  is  $j_r \approx 1.86 \cdot 10^{-2}$ .

#### b. Dephasing rate

Generalizing the procedure described in the above Subsection for recursion equations (S31), one can find critical value  $j_\phi = J_\phi/W$  by means of the same Eqs.(S32) but with  $F(x)$  function replaced by another function  $F_2(x)$  where

$$F_2(x) = \frac{1}{x} \ln \left\{ K^2 \iint_{-1/2}^{1/2} dh_1 dh_2 [J^4 \cdot f(h_1, h_2)]^x \right\} \quad (\text{S35})$$

where

$$f(h_1, h_2) = \frac{1}{(h_1 - h_2)^2} \left( \frac{1}{h_1} + \frac{1}{h_2} \right)^2 \quad (\text{S36})$$

Equations (S35,S36) can be derived along the line of ideas present in Refs. [69, 70]. We introduce Laplace transform  $G(e^{-x})$  of the probability density function  $\mathcal{P}(\Gamma_j)$  where evolution of  $\Gamma_j$  along the recursion follows Eq.(S31). Then, instead of Eq.(9) of Ref. [70] we come to

$$G_{L+1}(x) = \prod_{\mu=1}^{K(K-1)/2} \int \rho(\epsilon_\mu) d\epsilon_\mu G_L^2(x + \epsilon_\mu) \quad (\text{S37})$$

where  $\mu$  stays for a pair of indices  $j, m$  staying in the R.H.S. of Eq.(S31), number of such pairs is  $K(K-1)/2$ . Density of the distribution  $\rho(\epsilon) d\epsilon$  is determined by the original distribution of local fields  $P_0(h_1, h_2) = W^{-2}\theta(\frac{W}{2} - |h_1|)\theta(\frac{W}{2} - |h_2|)$  and by the function (S36) that corresponds to the  $h$ -dependent factor in Eq.(S31) after we set  $h_j \rightarrow 0$ , as it was done in the beginning of Sec. II A 1 above. Second power of the characteristic function  $G$  comes about in Eq.(S37) due to the presence of two random variables  $\Gamma_k, \Gamma_m$  in the R.H.S. of Eq.(S31). General properties of the characteristic function  $G(x)$  are the same as in the original approach [69, 70]. In particular, freezing transition point is determined by its far right asymptotics  $x \rightarrow \infty$  where  $1 - G(x) \equiv g(x) \ll 1$ , and thus  $G^2(x) \approx 1 - 2g(x)$ . Due to that fact, we

come to Eq.(S35), where we also replaced  $K(K-1) \rightarrow K^2$  in the large- $K$  limit.

Approximate integration in Eq.(S35) and use of (S32) gives

$$\frac{1}{j_c(2\sqrt{2}+2)^{1/2}} = eK \ln \frac{\sqrt{\alpha_1}}{j_c} \quad (\text{S38})$$

where  $\alpha_1 \sim 1$ . It follows from Eqs.(S38,S34) that  $j_\phi < j_r$  in general. For  $K = 3$  numerical integration in Eq.(S35) leads to  $j_\phi = 1.4 \cdot 10^{-2}$ . In a similar way, we find critical values  $j_r$  and  $j_c$  for several other branching numbers  $K$ , the results are summarized in the Table 1.

$K$	3	4	5	6
$j_r$	$1.86 \cdot 10^{-2}$	$1.24 \cdot 10^{-2}$	$0.92 \cdot 10^{-2}$	$0.72 \cdot 10^{-2}$
$j_c$	$1.4 \cdot 10^{-2}$	$1.0 \cdot 10^{-2}$	$0.8 \cdot 10^{-2}$	$0.6 \cdot 10^{-2}$

## 5.B. Account for self-energy correction

### a. Relaxation rate threshold

Much better analytical approximation was proposed for the problem that is very similar to the one defined by Eq.(S23), in Ref. [68]. They show that self-energy effects may be accounted for by the replacement of bare distribution  $P_0(h)$  by *effective* distribution function  $P_1(h)$

$$P_1(h) = \frac{1}{W - 4J^2/W} \theta\left(\frac{W}{2} - |h|\right) \theta\left(|h| - \frac{2J^2}{W}\right) \quad (\text{S39})$$

which accounts for the absence of too small resonance denominators in the R.H.S. of Eq.(S23), due to self-energy corrections. An important feature of the distribution (S39) is its symmetry:  $P_1(h/W) = P_1(W/h)$ . Due to this symmetry, one does not need to optimize over the value of exponent  $x$ , as it was done in Sec.2A above. It was shown already in Ref. [67] that the optimal exponent is now  $x = 1/2$ . Instead of two equations in Eq.(S32), we put  $x = 1/2$  into the definition of function  $F(x)$  in Eq.(S33) and use the second equation of Eqs.(S32) only:  $F_1(\frac{1}{2}) = 0$ . Then the critical value  $j_r = J_r/W$  can be found [68] from

$$KJ \int P_1(h) \frac{dh}{h} = 1 \quad (\text{S40})$$

Using Eq.(S39) we get then an algebraic equation

$$\frac{1}{2j_r} - 2j_r = 2K \ln \frac{1}{2j_r} \quad (\text{S41})$$

whose solution is  $j_r \approx 0.03$  for  $K = 3$  in very good agreement with numerical results [71] (agreement persists for other values of  $K$  as well).

### b. Dephasing rate threshold

Main idea for account of  $\text{Re } \Sigma$  is the same as in the above Subsection: we use  $x = 1/2$  and integrate over region on the plane  $(h_1, h_2)$  where  $|\text{Re } \Sigma| < W/2$  and also both  $|h_{1,2}| < W/2$ . Specifically, we need to solve

$$J^2 K^2 \int dh_1 dh_2 P_2(h_1, h_2) \left| \frac{1}{h_1} + \frac{1}{h_2} \right| \frac{1}{|h_1 - h_2|} = 1 \quad (\text{S42})$$

with renormalized distribution

$$P_2(h_1, h_2) = \frac{1+a}{W^2} \theta\left(\frac{W}{2} - |S|\right) \theta\left(\frac{W}{2} - |h_1|\right) \theta\left(\frac{W}{2} - |h_2|\right)$$

where

$$S \equiv \text{Re } \Sigma = J^4 \left( \frac{1}{h_1} + \frac{1}{h_2} \right)^2 \frac{1}{|h_1 - h_2|} \quad (\text{S43})$$

and  $a \ll 1$  accounts for the change of normalization of the distribution due to restriction  $|s| < W/2$ ; this is very small effect which can be neglected.

In dimensionless units (setting  $W = 1$  and changing  $J \rightarrow j$ ), we need to solve for the value of  $j$  the following equation (main interest is in  $K = 3$ ):

$$\int_{-1/2}^{1/2} \int_{-1/2}^{1/2} dx dy \left| \frac{1}{x} + \frac{1}{y} \right| \frac{\theta(\frac{1}{2} - |s|)}{|x - y|} = \frac{1}{j^2 K^2} \quad (\text{S44})$$

where

$$s = j^4 \left( \frac{1}{x} + \frac{1}{y} \right)^2 \frac{1}{|x - y|}$$

Numerical solution for  $K = 3$  leads to  $j_c = 0.02$ . Ratio  $j_r/j_c = 1.5$ . In a similar way, we find critical values  $j_r$  and  $j_c$  for several other branching numbers  $K$ , the results are summarized in the Table 2.

$K$	3	4	5	6
$j_r$	$3.0 \cdot 10^{-2}$	$1.95 \cdot 10^{-2}$	$1.4 \cdot 10^{-2}$	$1.1 \cdot 10^{-2}$
$j_c$	$2.0 \cdot 10^{-2}$	$1.3 \cdot 10^{-2}$	$1.0 \cdot 10^{-2}$	$0.75 \cdot 10^{-2}$

Results collected in Table 1 and Table 2 demonstrate that  $j_c < j_r$  for all various values of  $K$  and within two different approximation schemes.